AD-A105 856 GEORGE WASHINGTON UNIV WASHINGTON D C DEPT OF CHEMISTRY F/G 7/4
AUGER SPECTROSCOPY AS A PROBE OF VALENCE BONDS AND BANDS.(U)
OCT 81 D E RAMAKER N00014-80-K-8052
UNCLASSIFIED TR-7 NL

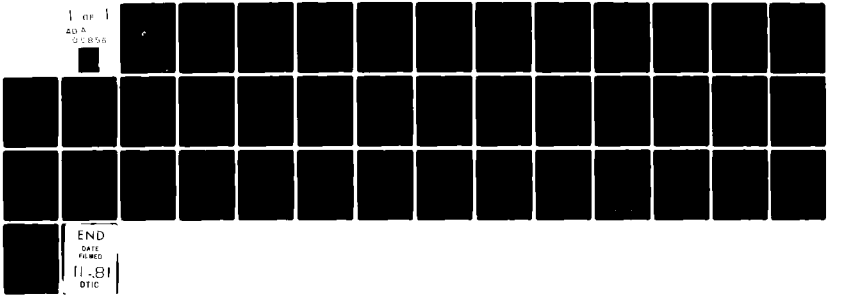

END
DATE FILMED
11-81
DTIC

OFFICE OF NAVAL RESEARCH

N00014-80-K-0852

Task No. 056-681

Technical Report No. 7

Auger Spectroscopy as a Probe of Valence Bonds and Bands

by

David E. Ramaker

Prepared for Publication

in the

Springer-Series in Chemical Physics, ISISS Proceedings

(Springer-Verlag)

George Washington University
Department of Chemistry
Washington, D.C. 20052

October 1981

SECURITY CLASSIFICATION OF THIS PAGE (When Data Entered)

REPORT DOCUMENTATION PAGE	READ INSTRUCTIONS BEFORE COMPLETING FORM
1 REPORT NUMBER: No. 7	2 GOVT ACCESSION NO. / 3 RECIPIENT'S CATALOG NUMBER
4 TITLE (and Subtitle): Auger Spectroscopy as a Probe of Valence Bonds and Bands	5 TYPE OF REPORT & PERIOD COVERED: Technical Report / 6 PERFORMING ORG. REPORT NUMBER
7 AUTHOR(s): David E. Ramaker	8 CONTRACT OR GRANT NUMBER(s): N00014-80-K-8052
9 PERFORMING ORGANIZATION NAME AND ADDRESS: Chemistry Department, George Washington University, Washington, D.C. 20052	10 PROGRAM ELEMENT, PROJECT, TASK AREA & WORK UNIT NUMBERS: Prog. Elem. No. 61153N; Task Area No. PP 013-08-01; Work Unit No. NR 056-681
11 CONTROLLING OFFICE NAME AND ADDRESS	12 REPORT DATE: October 1981 / 13 NUMBER OF PAGES: 79
14 MONITORING AGENCY NAME & ADDRESS (if different from Controlling Office)	15 SECURITY CLASS. (of this report): Unclassified / 15a DECLASSIFICATION/DOWNGRADING SCHEDULE

LEVEL

16 DISTRIBUTION STATEMENT (of this Report)

This document has been approved for public release and sale; its distribution is unlimited.

17 DISTRIBUTION STATEMENT (of the abstract entered in Block 20, if different from Report)

18 SUPPLEMENTARY NOTES

Submitted for publication in the Springer Series of Chemical Physics, ISISS Proceedings (Springer-Verlag)

19 KEY WORDS (Continue on reverse side if necessary and identify by block number)

Auger electron spectroscopy, screening, localization, atomic matrix elements, electron and photon stimulated desorption,

20 ABSTRACT (Continue on reverse side if necessary and identify by block number)

The use of Auger spectroscopy as a probe of valence bonds and bands is reviewed. A one-electron lineshape description is outlined. The determination of atomic Auger matrix elements and the question of local vs. Mulliken populations is fully examined. The many body effects of localization and screening are shown to be important. The outlook for Auger spectroscopy in electronic structure determination in the gas phase, at a chemisorbed layer, at an interface, or in the bulk is indicated. Also included is a discussion of the role

DD FORM 1 JAN 73 1473 EDITION OF 1 NOV 65 IS OBSOLETE S/N 0102-014-6601 | Unclassified SECURITY CLASSIFICATION OF THIS PAGE (When Data Entered)

Auger spectroscopy can play in the elucidation of the electron or photon stimulated desorption (ESD/PSD) mechanism.

AUGER SPECTROSCOPY AS A PROBE OF VALENCE BONDS AND BANDS

David E. Ramaker*
Chemistry Department
George Washington University
Washington, D. C. 20052

*Supported by the Office of Naval Research

Abstract

The use of Auger spectroscopy as a probe of valence bonds and bands is reviewed. A one-electron lineshape description is outlined. The determination of atomic Auger matrix elements and the question of local vs. Mulliken populations is fully examined. The many body effects of localization and screening are shown to be important. The outlook for Auger spectroscopy in electronic structure determination in the gas phase, at a chemisorbed layer, at an interface, or in the bulk is indicated. Also included is a discussion of the role Auger spectroscopy can play in the elucidation of the electron or photon stimulated desorption (ESD/PSD) mechanism.

Outline

I. Introduction

For almost a decade now, Auger Electron Spectroscopy (AES) has been utilized as a technique for elemental identification and trace analysis at the surface of solids (1). Indeed over these years AES has become a widely available and almost indispensable technique for determining surface cleanliness, surface coverage and even depth profiling. More recently, the Auger lineshape has been recognized as a source of chemical and electronic structure information. Just how this information can be extracted from the Auger lineshape requires a thorough understanding of the factors contributing to the Auger process. This review will examine several of these factors.

It is often true that one decides to write a review (or one requests that someone else write a review) when he perceives that significant progress has occurred recently in an area. Thus, from the seven review articles written in the last two years on AES, one might conclude that significant progress has been achieved recently in our understanding of the Auger process. I believe this is indeed the case. Table 1 summarizes these seven review articles and includes the article of Crasemann (2) (unpublished lecture notes) for completeness. The principle topics reviewed indicate the breath of the recent progress and also the relatively small overlap in subject matter between these eight articles. Holloway's review (1) of experimental approach and applications also covers the sometimes difficult but

important task of extracting a nearly quantitative Auger lineshape or spectrum from the experimental data. This aspect will not be covered here; I refer the reader to the Holloway article as well as to some of the original work in this area (4,5). The reviews by Larkins (6) and Madden (7) concentrate on the chemical information contained in the Auger energies; this important topic also will be omitted from this review. The works by Moddeman (8), Aksela (3), and Crasemann (2) concentrate on the Auger effect in atoms and molecules in the gas phase, and as such also will not be considered here. The reviews by Kleiman (9) and Fuggle (10) have the g :atest potential overlap with this work since screening and localization effects on the Auger lineshape will be considered here also. However the results and conclusions presented here on screening do not appear in their reviews; the concept of localization is extended beyond the elemental metals and alloys they consider. The emphasis here will be on AES as a probe of the valence density of states (DOS) with applications to metals, insulators, and molecules.

The Auger process is a two electron process, which makes it unique from the more common one-electron processes such as are involved in x-ray and photo emission (XES and PES). These three spectroscopies are illustrated in Fig. 1 for the case of an atom involving the K and L shells. The Auger and x-ray emission processes may be initiated by either an incoming electron or photon, the photo emission process of course only by a photon. The Auger

and x-ray emission processes compete to fill the core hole; however, the Auger process clearly dominates for core levels with binding energies less than 5000 eV (11). Also illustrated is the shake-off process, a process which always occurs with some probability during an ionization event and results from relaxation of the atom in the presence of the core hole. A subsequent Auger event (a subsequent x-ray emission event may also occur) results in a shake/Auger satellite; i.e., Auger electron contributions generally shifted down in energy from the parent Auger contributions. The parent and satellite contributions are termed in this example the K-LL and KL-LLL transitions on the basis of their initial and final state hole configurations.

One may be lead to question the appropriateness of AES as a probe of valence band information. Why bother with AES when XES and PES provide the one electron DOS, N(E), more directly? The final state of the Auger and shake/Auger events as illustrated in Fig. 1 leaves the system with 2 or 3 valence holes compared with 1 valence hole in XES and PES. This tends to complicate the spectrum analysis because of the increase in possible final state hole configurations. As a first approximation, the CVV (core-valence-valence) Auger lineshape A(E) is a fold of N(E) (9),

$$A(E) = \int N(E-\varepsilon)\ N(\varepsilon)\ d\varepsilon\ . \qquad 1)$$

However Table 2, which compares some features of XES and PES with AES, indicates the greater surface sensitivity of AES compared with XES, and the site specificity of the valence DOS probed by

AES compared with the all sites DOS probed by PES (12,13). The lack of surface sensitivity in XES arises from the large escape depth of the observed outgoing photons. AES and XES probe the DOS only near the initial core hole; no initial core hole exist in PES. The combined surface sensitivity and site specificity offer unique advantages for AES. This along with the wide availability of AES instrumentation (1) makes it an attractive technique for electronic structure studies.

II. Lineshape description - one electron model

A detailed interpretation of the Auger lineshape requires a quantitative description of each Auger transition. Each transition may be characterized by an Auger energy, width, and intensity. These may be simply expressed in terms of the initial and final state holes in a one-electron orbital model (14):

$$E_{cxy} = E_c - E_x - E_y - U_{xy} \qquad 2)$$

$$\Gamma_{cxy} = \Gamma_c + \Gamma_x + \Gamma_y + 2K_{xy} \qquad 3)$$

$$I_{cxy} = 2\pi/\hbar\ |\langle \Psi_f | H-E | \Psi_i \rangle|^2 \approx \sum_{nm} c_{xn}^2 c_{ym}^2 P_{cnm} \qquad 4)$$

E_c and Γ_c are the binding energy and width of the initial core hole; Γ_c includes the lifetime broadening and spin-orbit splitting contributions. The final valence state holes have the binding energies E_x and E_y and widths Γ_x and Γ_y; the widths in this instance include solid state banding effects and nuclear (vibrational) effects (15). These one electron parameters may be obtained from ab initio calculations (15) but most often are

obtained empirically (14). This is consistent with the desire to make the Auger lineshape interpretation techniques generally practical, available to a large number of experimentalist in the field and applicable to a large number of interesting systems. Binding energies are best obtained from XPS, the widths from either XES or UPS data (14).

The quantities U_{xy} and K_{xy} reflect the presence of two holes in the final state. U_{xy} is the effective hole-hole Coulomb repulsion, K_{xy} is the singlet-triplet splitting which is assumed to be unresolved in the solid. They may be defined in a LCAO-MO picture (e.g. $X = \sum_n c_{xn} f_n$) by the expressions (utilizing the zero differential overlap (ZDO) approximation)

$$U_{xy} = \langle XY | r_{12}^{-1} | XY \rangle = \sum_{nm} c_{xn}^2 c_{ym}^2 \; U_{nm} \qquad 5)$$

$$K_{xy} = \langle XY | r_{12}^{-1} | YX \rangle = \sum_{nm} c_{xn} c_{yn} c_{xm} c_{ym} \; U_{nm} \; , \qquad 6)$$

where the atomic repulsion integrals must reflect the screening and relaxation of the atom,

$$U_{nm} = \langle f_n f_m | r_{12}^{-1} | f_n f_m \rangle = f(n,m) - r_n \; \delta_{nm} \; . \qquad 7)$$

Here f(n,m) are the atomic repulsion integrals and r_n is a "static relaxation energy"(16). The one center integrals f(n,m) may be obtained from the integral tables of Mann (17) and the two center f(n,m) from some suitable interpolation scheme (18). The quantities r_n have been determined empirically by Shirley (16) from atomic Auger spectra.

In the rigid one-electron model, the expression for the Auger intensity reduces to a two electron matrix element (see

Sec. IV). In the LCAO-MO picture it reduces still further to a sum over terms involving the atomic populations and an atomic Auger matrix element, P_{cnm} (eq. (4)). Assuming P_{cnm} is large only when f_n and f_m are orbitals on the atom with the core hole (see Sec. II.B), the sum in eq. (4) often reduces to a single term, $c_{x\ell}^2 \, c_{y\ell'}^2 \, P_{c\ell\ell'}$, which involves the square of the local populations (with local angular momentum ℓ or ℓ') on the initial core hole site. The Auger lineshape which involves a sum over the Auger transitions,

$$A(E) = \sum_{xy} c_{x\ell}^2 \, c_{y\ell'}^2 \; P_{c\ell\ell'} \qquad 8)$$

is then closely approximated by a fold over the DOS (eq. (1)) on the core hole site (site specificity), albeit modulated by the different atomic Auger matrix elements $P_{c\ell\ell'}$, (e.g. P_{css}, P_{csp} or P_{cpp}; s or p giving the local angular momentum).

Eqs. (2) through (8) describe the Auger lineshape, but several basic questions remain. What electron density is actually probed by the Auger process? Are the $c_{x\ell}^2$ in eq. (8) best given by the local or Mulliken populations? Does the Auger lineshape reflect an initial screened core hole DOS or the final DOS? Are the final state holes localized on an atom, a molecular cluster on throughout the solid (i.e. are the DOS probed atomic like, molecular like, or band like)? Finally, what is the best way to determine the Auger matrix elements $P_{c\ell\ell'}$? These questions will be examined in Secs. II. B through IV. A review of the outlook for AES will be given in Sec. V.

A. Atomic Auger matrix elements

Atomic Auger matrix elements have been calculated for much of the periodic table within a one electron Hartree Fock Slater approximation by McGuire (19,20) and Walters and Bhalla (21,22). Their results are compared with experimental date in Figs. 2 and 3 for low atomic number Z(23). Fig. 2 compares results for the KLL transitions, Fig. 3 for $L_{23}MM$. The matrix element per filled shell, $P_{c\ell\ell'}$ (i.e. s^2, p^6, or d^{10} etc.) is plotted; $P_{c\ell\ell'}$ is defined by the expressions (24)

$$P_{c\ell\ell} = \frac{(4\ell+2)(4\ell+1)}{(4\ell+2-n)(4\ell+1-n)} \times (P_{c\ell\ell})_{act.} \qquad 9)$$

$$P_{c\ell\ell'} = \frac{(4\ell+2)}{(4\ell+2-n)} \times (P_{c\ell\ell'})_{act.} \qquad 10)$$

where n is the number of holes in the ℓ shell and $(P_{c\ell\ell'})_{act.}$ is the actual Auger matrix element or experimental intensity. (It is assumed the ℓ' shell in eq. (10) is filled.) Since generally one is interested only in the relative $P_{c\ell\ell'}$ intensities, they have been normalized such that P_{cpp} is 100 for all Z. The theoretical results of McGuire and Walters and Bhalla have been scaled to the experimental results of the inert gases; this required scale factors (ranging from .59 to 2.06) significantly different from 1. These scale factors reflect the magnitude of the errors in the one-electron results. Electron correlation effects at the atomic level are clearly very important. The configuration interaction (CI) results of Chen and Crasemann

(25,26) include electron correlation; their unscaled results agree closely with the experimental.

Figs. 2 and 3 reveal three very important points. 1) The variation of the relative Auger matrix elements with atomic number is rather small. 2) What variation does exist is predicted remarkably well by the *scaled one-electron results*. This indicates the large correlation error is rather constant with Z. 3) Both atomic gas phase, molecular phase, and solid phase experimental data is given, no systematic differences between this data exist. This is true even for the dd, pd, and pp matrix elements of the transition metals where electron screening in the solid (Sec. IV) is expected to cause significant changes. Recently Vayrynen (27) suggested that the relative atomic matrix elements for solid Mn are very different from those in the gas phase. However Vayrynen's results are inconclusive because of an inadequate background removal procedure in the solid phase. Clearly more careful work needs to be done to check this important question. For the present, the results of Figs. 2 and 3 suggest that gas phase atomic data or the <u>scaled</u> one-electron results can be utilized for interpretation of Auger lineshapes in the solid.

B. Local or Mulliken populations

The question of whether the Auger process probes the local or Mulliken populations arises from our use of eq. (8). Use of eq. (4) would automatically weight the DOS in the proper manner.

However this question is of general chemical interest in any event. Does the Auger process in any way sample the bonding charge? The local and Mulliken populations are defined by the M.O. overlap equation,

$$\sum_{nm} c_n c_m S_{nm} = \sum_n \left(c_n^2 + \sum_{m \neq n} c_n c_m S_{nm} \right) = 1, \qquad 11)$$

where $S_{nm} = \langle f_n | f_m \rangle$ is the atomic overlap. The Mulliken populations include the "bonding" charge such that

$$P_n^M = c_n^2 + \frac{1}{2} \sum_{m \neq n} c_n c_m S_{nm}, \qquad 12)$$

and satisfy the sum rule

$$\sum_n P_n^M = 1. \qquad 13)$$

The local populations include only the diagonal terms $P_n^L = c_n^2$.

An analysis of the Auger matrix element by Hutson et al. (30) gives for a two atom system with atoms a and b (i.e. X= $af_a + bf_b$ with core hole site 'a' the result,

$$I^{Ex} = a^4 M_{caa}^2 + a^3 b (M_{cab} + M_{cba}) M_{caa} + \ldots \qquad 14)$$

It was assumed that $M_{abb} < M_{cab}$, $M_{cba} < M_{caa}$ since inter-atomic Auger matrix elements $M_{cab} = \langle \phi_c \phi_K | r_{12}^{-1} | f_a f_b \rangle$ are generally much smaller than intra-atomic elements, $M_{caa} = \langle \phi_c \phi_K | r_{12}^{-1} | f_a f_a \rangle$ (31). The use of local populations,

$$I^L = (P_a^L)^2 M_{caa}^2 = a^4 M_{caa}^2, \qquad 15)$$

is valid provided all inter-atomic elements are indeed negligible. The use of Mulliken populations gives the result

$$I^M = (P_a^M)^2 M_{caa}^2 = (a^2 + abS)^2 M_{caa}^2 \qquad 16)$$

$$I^M = a^4 M_{caa}^2 + 2a^3 bS M_{caa}^2. \qquad 17)$$

The second terms in eqs. (17) and (14) are equivalent if $(M_{cab} + M_{cba})/M_{caa} = 2S$. A semiempirical analysis by Matthews and Kominos (31) indicates that $(M_{cab} + M_{cba})/M_{caa} \sim 10^{-2}$. Typical two center overlaps $S = \langle f_a | f_b \rangle \sim 10^{-1}$, indicating the second terms in general are not equivalent.

The above analysis suggest the result $I^L < I^{Ex} < I^M$ at the bottom of a band when S>0; $I^L > I^{Ex} > I^M$ at the top of a band when S<0. However one expects some orbital contraction (expansion) at the bottom (top) of a band relative to the free atom. This would have the effect of moving I^{Ex} in the direction of I^M and away from I^L, but no clear answer as to whether I^M or I^L is closer to I^{Ex} comes from this analysis.

Comparison with experiment is equally inconclusive. Jennison (32) first noted for the Si $L_{23}VV$ lineshape of elemental Si that $I^L \approx I^{Exp} \neq I^M$. However for the Si $L_{23}VV$ lineshape in Pd_4Si (33) and at the Pd/Si interface (34), it was found that $I^M \approx I^{Exp}$. For the N KVV lineshape of the NO_3 oxyanion (30), a similar result was observed (i.e. $I^M \approx I^L \approx I^{Exp}$). Obviously more work is necessary here. At present it seems reasonable to utilize the more convenient Mulliken populations, particularly in a multiband lineshape when the bonding charge does not dominate in any region of the spectrum (e.g. such as in the N KVV of NO_3). In a single band lineshape where the bonding charge dominates some part of the spectrum, the local populations may be preferred (e.g. such as in the Si $L_{23}VV$ of elemental Si (32)).

III. Localization

In the Cini-Sawatzky (35) model of the Auger process in elemental solids, two parameters determine the degree of localization of the CVV two-hole final state. If the effective Coulomb repulsion U^e_{VV} is large compared to the bandwidth ($U^e_{VV} > \Gamma$), the lineshape will be atomic like, if $\Gamma > U^e_{VV}$ the lineshape will be band like. In systems where $U^e_{VV} \approx \Gamma$ both atomic and band like contributions are evident in the lineshape (i.e., correlation effects are important).

The results of Cini and Sawatzky were obtained from utilizing the Anderson and Hubbard many body models. The equations which enter are solvable only for the initially filled band or two-hole final state. Some work has been reported for the initially unfilled band (36), but the initial conclusions of Cini and Sawatzky do not appear to be substantialy altered.

The Cini-Sawatzky results can be simply understood by considering a cluster LCAO-MO-CI approach (18). For the moment consider a simple two-orbital system which has two holes present resulting from the Auger process in an initially filled state (18,37). The holes can be described by the one electron atomic orbitals f_a^2 and f_b^2 with binding energy ϵ giving the Hamiltonian matrix as below:

$$\begin{array}{c|ccc} & f_a^2 & f_b^2 & \frac{1}{\sqrt{2}}(f_af_b + f_bf_a) \\ \hline f_a^2 & 2\epsilon + U_{aa} & 0 & H_{ab} \\ f_b^2 & 0 & 2\epsilon + U_{aa} & H_{ab} \\ \frac{1}{\sqrt{2}}(f_af_b + f_bf_a) & H_{ab} & H_{ab} & 2\epsilon + U_{ab} \end{array} , \qquad (18)$$

where $U_{aa} = \langle f_a^1 | r_{12}^{-1} | f_a^2 \rangle$, $U_{ab} = \langle f_af_b | r_{12}^{-1} | f_af_b \rangle$, and $H_{ab} = \sqrt{2}\langle f_a | H | f_b \rangle$ ($H_{ab} \propto \Gamma$ in the solid). Clearly if $H_{ab} < U_{aa} - U_{ab}$, very little mixing occurs and the hole states f_a and f_b properly describe the localization of the two holes. In this instance the Auger lineshape is atomic like probing only the two-electron eigenstate f_a^2 (core hole site). If $H_{ab} > U_{aa} - U_{ab}$, the mixing of the configurations is complete and the linear combinations $f_a \pm f_b$ properly describe the localization of the holes. As such, the lineshape is molecular like (band like for the solid) sampling the eigenstates $1/2\,(f_a + f_b)^2$, $1/\sqrt{2}\,(f_a + f_b)(f_a - f_b)$ and $1/2\,(f_a - f_b)^2$ and giving relative Auger intensities 1/4, 1/2, and 1/4 respectively. If $H_{ab} \approx U_{aa} - U_{ab}$, of course intermediate mixing occurs giving both contributions.

Fig. 4 compares the bandwidth Γ_{nd} with U^e_{ndnd} for the metals with electron configurations d^6s^2 to $d^{10}s^2p^2$. For all three rows of this series the Γ and U^e plots cross in the region d^8s^2 to $d^{10}s$. The Auger lineshapes of these "transitional" metals are given in Fig. 5 and compared with a fold of the DOS, N X N (36,9), and in some instances the calculated atomic like Auger lineshape. The lineshape for Cu is clearly atomic like (28, 38-41), that for Ag is also, although some controversy has occurred in the literature concerning this question (42-46). The lineshape for Au appears to be band like although shifted down in energy by 5 eV (47,48). The Ni (49,9) and Pd (9,50) lineshapes show atomic like and band like contributions separated by 3 to 4 eV, but no multiplet structure is evident. These lineshapes

indicate the rather smooth transition from atomic to band like character. The d^2s^2 to d^7s^2 metals are clearly band like (51,52), the $d^{10}s^2$ to $d^{10}s^2p^2$ metals atomic like (53).

Recently Dunlap et al. (37) showed that intermediate levels of localization can exist, i.e. localization on some sub-cluster of the system. The systems studied were NO_3^-, $SO_4^=$, and SiO_2. The pertinent parameters are schematically illustrated in Fig. 6. The degree of localization can best be summarized as follows:

$$\begin{array}{lll} V < U_{AA} - U_{AO} = U^e_{AA} & & \phi \rightarrow AO \\ \nu > U^e_{AA'} & \gamma < U_{AA} - U_{AA'} = U^e_{AA} & \phi \rightarrow LO \\ \gamma > U^e_{AA} & \Gamma < U_{VV} - U_{VV'} = U^e_{VV} & \phi \rightarrow MO \\ \Gamma > U^e_{VV} & & \phi \rightarrow BO \end{array} \qquad (19)$$

where AO, LO, MO, and BO refer to atomic, lobe like, molecular, and band like orbitals respectively. The results plotted in Fig. 6 indicate that the two-hole final state is best represented by NO_3^- and $SO_4^=$ MO's, and a Si-O-Si LO. Also plotted in Fig. 6 is $U^e_{AA'}$, the effective lobe orbital three hole repulsion energy appropriate for the final state resulting from the shake/Auger process as discussed in Sec. I. The three hole final state is best represented by a NO_3^- MO and S-O and Si-O-Si LO's.

The experimental Auger lineshapes verify these conclusions (37). Fig. 7 compares the experimental N KVV lineshape for NO_3^- with that predicted theoretically from a semi-empirically derived one-electron NO_3^- M.O. DOS (30). The energy separation between

the principle peak of the parent and shake/Auger contributions (ΔE, see Sec. IV) is predicted to be -6eV utilizing a NO_3^- MO for both the two and three hole final states. Experimentally the best fit is obtained with ΔE=-5eV. Fig. 8 compares the experimental and theoretical S $L_{23}VV$ lineshapes for $SO_4^=$ (37,56), again utilizing a $SO_4^=$ MO DOS to determine the theoretical lineshape. ΔE is predicted to be -8 or -2eV depending on whether one uses the MO or LO orbitals for the three-hole final state. Experimentally the best fit is obtained with $\Delta E \simeq$-2eV verifying the appropriateness of the LO three hole final state of $SO_4^=$.

Fig. 9 compares the experimental and theoretical (without the shake/Auger contributions in this case) O KVV and Si $L_{23}VV$ lineshapes in SiO_2 (57,14,37). The theoretical Si $L_{23}VV$ lineshape was first determined from a SiO_4^{4-} MO giving the difference curve in Fig. 9d (57,14). The peaks centered at 55 and 68eV were attributed to shake/Auger satellites, the peak at 84eV to beam damage. Later electron correlation was included via a CI calculation allowing for localization on the Si-O-Si LO's (18). These results are indicated by the bars in 9c, the dotted bars the Si-O-Si localized contributions, the solid bars the completely delocalized (band like) contributions. Notice the localized contributions now account for the intensity originally attributed to the shake/Auger contributions. The shake/Auger satellites may in fact not contribute because the shake hole may not remain localized to the core hole. Recently Jennison (58) suggested electron

screening of the final state holes is important in decreasing $U^e_{\underline{XY}}$, thus aiding hole *delocalization*. *However, screening will* decrease U^{Σ}_{CV} even more than $U^e_{\underline{XY}}$ so that localized contributions *may still contribute some measure* of intensity to the lineshape, but shake/Auger satellites may not.

The O KVV lineshape in SiO_2 was theoretically evaluated assuming initially a totally localized Si-O-Si final state (Fig. 9a.). The difference peaks around 475 and 495eV have been attributed to shake/Auger satellites, the peak at 510eV to delocalized contributions dominated by the O 2p non-bonding orbitals. Results of an LCAO-MO-CI calculation on a 16 O atom cluster in a tetrahedral SiO_2 lattice utilizing a parameterized Hamiltonian (18) is indicated in Fig. 10. It illustrates the transition from localized to non-localized lineshape behaviour as a function of U/Γ . *A 20% nonlocal intensity separated by ≈7eV from the local* peak as indicated by the O KVV lineshape (Fig. 9b) gives a U/Γ of 2.5 (Fig. 10, $U_{ij} \neq 0$). Since the oxygen atom hole-hole repulsion is 10-15eV, this corresponds to an oxygen non-bonding band width of 4 to 6eV in SiO_2, in reasonable agreement with theory and experiment (18).

Fig. 10 shows clearly a point which needs further emphasis here. The transition from the band like to the atomic like lineshape is relatively sharp and occurs at $U/\Gamma \approx 1$, not at $U/\Gamma = 2$, where Γ = the <u>full</u> bandwidth. This is in agreement with the results of Sawatzky and Lenselink (59) *utilizing the Hubbard model*

for an infinite system. There is much confusion in the literature on this point, (note Fig. 4 plots Γ , others have plotted 2Γ (40, 6,9,10)) probably because in the original paper, Cini (35) apparently defined W to be the <u>half</u> bandwidth giving the criterion U>2W. Sawatzky defined W to be the full bandwidth, but still used *the criterion* U>2W because his initial paper (35) utilized a simplifying approximation to his exact solution valid only for U>2W. The point of steepest slope in the transition occurs at $U/\Gamma = 1.0 \pm .2$ (59) depending on the crystal structure. The transition becomes less sharp and occurs at different values of U/Γ for smaller systems (e.g. $U/\Gamma \approx 1.2$ *for diatomic molecules* (18,37)).

Another important point concerns the energy separation ΔE between the two contributions. Fig. 10 shows that the shift ΔE of the atomic like peak from the zero point energy (middle of band when U=0) is greater than U in agreement with Sawatzky and Lenselink (59). However the band like portion of the spectrum is also skewed to lower energies with increasing U/Γ . Fig. 10 indicates the shift ΔE between the <u>*centroids*</u> of the two contributions is less than U. Fig. 10 shows results for two cases; assuming two center integrals $U_{ij}=0$ and $U_{ij}\neq 0$. The calculation of Sawatzky and Lenselink within the Hubbard model makes the necessary approximation $U_{ij}=0$. The effect of $U_{ij}\neq 0$ is to reduce the effective value of U(i.e. $U^e \approx U-U_{ij}$) as indicated by the asymptotic approach of ΔE to U^e and the transition at $U/\Gamma \approx 1.7$

(equivalent to $U^e/\Gamma \simeq 1$) in this instance. Thus as shown, the separation between the two contributions slightly <u>underestimates</u> U^e and significantly underestimates U.

IV Screening

Electron screening of the core hole alters the Auger lineshape in two ways: 1) it introduces shake/Auger satellites as previously discussed, and 2) it changes the parent Auger contribution (60). Consider the core ionization process initiating the Auger process. It's rate r_{ion} is given by the expression (61),

$$r_{ion} = 2\pi/\hbar \sum_m |\langle \phi_c \psi^G | \hat{T} | \varepsilon_\lambda \psi^i_m \rangle|^2 \qquad 20)$$
$$= 2\pi/\hbar \langle \phi_c | \hat{T} | \varepsilon_\lambda \rangle \langle S_n^2 + \sum_{m=SU} S_m^2 + \sum_{m=SO} S_m^2 \rangle,$$

where $\phi_c \psi^G$ is the ground state before the ionization process, $\varepsilon_\lambda \psi^i_m$ is the initial Auger state relaxed in the presence of the core hole, $\hat{T}$ is the appropriate ionization operator, $S_m = \langle \psi^G | \psi^i_m \rangle$, and SU and SO denote shake-up and shake-off contributions respectively. The shake-off contributions generally result from atomic relaxation of the core hole site (62), they produce the Auger satellites with lineshape characteristics (57,30),

$$I_{cs-svv'} = \frac{S_s^2}{(1 - \sum_s S_s^2)} \; W_s \; I_{cvv'} \qquad 21)$$

$$\Delta E_{cs-svv'} = U^e_{cs} - U^e_{sv} - U^e_{sv'} \qquad 22)$$

$$\Gamma_{cs-svv'} \simeq \Gamma_{cvv'} . \qquad 23)$$

In eqs. (21-23) 's' represents the shake electron, $I_{cvv'}$, ($\Gamma_{cvv'}$) the parent Auger intensity (width), W_s a statistical weight (57)

and U_{cs} and U_{sv} the Coulomb repulsion between the initial core-shake and final valence-shake holes respectively. S_s can be determined from the sudden approximation (57),

$$S_s^2 = \left(1 - \left[1 - c^2_{sq} + c^2_{sq} (1-P_a)^{1/2n}\right]^{2n}\right), \qquad 24)$$

where P_a is the atomic shake-off probability (63) and c^2_{sq} is the popul ation of the 's' MO on the core hole site. In eq. (20), the shake-up contributions normally result from charge transfer to the core hole site (62). They generally cause an Auger satellite of smaller intensity and energy shift and thus may be included theoretically with the parent contribution.

Shake/Auger satellites of up to 30-40% of the total intensity are clearly resolved in the gas phase spectra of the inert gases (64,65) and in molecules (66-68). In the solid phase, they have been found to significantly alter the experimental Auger lineshape of some metals (38,40,69) and insulators (70) (see Figs. 7,8, and 9). For quantitative Auger lineshape interpretation, they should not be ignored.

An understanding of the effect of screening on the parent Auger transitions can be gained from the Final State Rule (FS). A FS rule was first proposed by von Barth, Grossman (71) and Mahan (72) for the x-ray and photo-emission one-electron processes. Later Davis and Feldkamp (73) proposed an "Orthogonalized" FS (OFS) rule for the same processes. Recently the FS and OFS rules have been extended to the two electron Auger process (61).

Basically the FS and OFS rules are reductions of the many electron matrix element $\langle \Psi^i | r_{12}^{-1} | \Psi^f \rangle$ (for a single band system) to different two-electron integrals (61)

$$\text{FS:}\quad I_{ij} = 2\pi/\hbar |\langle ls\vec{k} | r_{12}^{-1} | \phi_i \bar{\phi}_j \rangle|^2 + O[S_{nf}(\bar{s}' + \rho')] \qquad 25)$$

$$\text{OFS:}\quad I_{ij} = 2\pi/\hbar |\langle ls\vec{k} | r_{12}^{-1} | \tilde{\phi}_i \tilde{\bar{\phi}}_j \rangle|^2 + O[S_{nf}\ \bar{s}'] \qquad 26)$$

where ϕ_i and $\bar{\phi}_j$ describe the final valence holes created by the Auger process (i.e. potential with no corehole), and $\tilde{\phi}_i$ and $\tilde{\bar{\phi}}_j$ are final state orbitals orthogonalized to the existing initial state valence holes,

$$\tilde{\phi}_i = \phi_i - \sum_{\varepsilon_m > \varepsilon_f} S_{mi}\, \phi'_m \qquad 27)$$

(ϕ'_m are initial orbitals relaxed in the presence of the core hole). The error terms contain $S_{nf} \propto 1/(\varepsilon_n - \varepsilon_f)$ (ε_f the Fermi energy, ε_n =min ($\varepsilon_i, \varepsilon_j$) the valence binding energy of the lower bound Auger hole) indicating the increased accuracy of the FS and OFS rules away from the Fermi level. $\bar{s}'$ and ρ' denote an effective average of the initial DOS and the integrated unoccupied DOS respectively. In general $\bar{s}' < \rho'$ indicating the increased accuracy of the OFS rule near the Fermi level. In the absence of configuration mixing (final state localization) basic sum rules (74) also indicate that the intensity of the individaul angular momentum contributions are determined by the initial state. Thus the intensities of the FS and OFS rules are normalized to that given by the initial state (e.g. $I^{\ell\ell'}_{OFS} = I^{\ell\ell'}_{FS} = I^{\ell\ell'}_{initial}$, $\ell\ell'$ = ss, sp, pp, etc.).

The results of the FS and OFS rules can be summarized in three statements: 1) the shape of the individual $\ell\ell'$ Auger contributions are determined by the final DOS, 2) the relative $\ell\ell'$ Auger intensities are determined by the initial state, and 3) the OFS rule is significantly different from the FS rule only near the Fermi level. As stated, the FS rule for the CVV band like Auger lineshapes, and as previously stated for x-ray and photoemission (71-73), indicate that XES, UPS, and AES probe an unscreened DOS. Thus they complement each other in electronic structure determinations. The limitation to CVV band like Auger lineshapes must be emphasized. A CCV Auger lineshape reflects a screened DOS because of the final state core hole (75). An atomic (localized) Auger lineshape does not reflect the band like DOS in any case. The Auger energy may however reflect a screened valence hole (e.g. the valence s electrons screen the localized 3d holes in the Cu $L_{23}M_{45}M_{45}$ Auger final state (9,76)).

Several applications of the FS rule to experimental data can be given illustrating its validity. Table 3 contains data for the O_2 O KVV (15), the C_2H_6 C KVV (77), and the NO_3 N KVV (30,61) lineshapes. It compares relative intensities of various transitions as determined from the initial state (relaxed in the presence of the core hole), from the final state (no core hole), and from either experiment or a more complete theory. (Fig. 11 also compares these data for NO_3^- (30,61)). Since the transitions listed in Table 3 are dominated by pp contributions, the better

agreement with the final state results indicates the validity of statement 1 above. Statement 2 is best illustrated by examing the Be KVV (77), Fig. 12 and Cu M_1VV (78) Auger lineshapes, Fig. 13. The individual L^2 Auger lineshapes have been determined from the theoretical final DOS; the relative L^2 intensities determined from the final and initial DOS respectively (assuming complete s electron screening) as indicated. 's' electron screening in metals has been indicated experimentally upon examing the CCV lineshapes in Si, Al, and Mg (75).

The utility of the OFS rule near the Fermi level (statement 3) has been illustrated for the intercalated graphite systems C_6Li and C_8Cs. Fig. 14 compares the DOS as obtained from UPS and from an interpretation of the C KVV Auger lineshape (80). The enhanced intercalant intensity in the Auger derived DOS can be attributed to electron screening of the initial core hole site within the OFS rule. Dunlap et al. (81) have compared the initial, final, and OFS rule transition ρ_π DOS as obtained from a 109 atom cluster using a parameterized SCF Hamiltonian. The OFS rule transition DOS is essentially the same as the final DOS, however with a much enhanced "intercalant peak," in qualitative agreement with the Auger derived DOS.

V. Outlook

The outlook for AES as a probe of valence DOS information is obviously good. Three main areas are briefly reviewed here: 1) the utilization of AES in understanding the mechanisms involved in electron and photon stimulated desorption (ESD/PSD) in covalent systems, 2) the utility of AES in the gas phase and possibly in the future for chemisorbed systems, and 3) the utilization of AES in gaining valuable electronic structure information in solids and at interfaces.

A. ESD/PSD

The role of the Auger process for desorption from highly ionic systems is reasonably well understood within the Varley mechanism (82) as proposed by Knotek and Feibelman (83). Although the Auger process has been demonstrated to be of importance in desorption from (or bulk beam damage of) covalent systems, its role is not as clear (84-89). Recently Ramaker, White and Murday (90) proposed and quantified a model for Auger (or for any process creating two valence holes) induced desorption from covalent (or ionic) systems.

Consider damage to surfaces where the surface atom or cluster is taken to be covalently bonded to a similar neighboring atom or cluster. For definiteness, consider a surface atom, S, covalently bonded via bonding orbital b_o to a single bulk atom, B, with bond energy D. The Auger process resulting from a core hole in S or B can leave the system initially in the repulsive state b_o^{-2}, with excitation energy $2E_b+U$, where E_b is the one-electron binding energy of b_o and U is the Coulomb interaction energy resulting from two holes in b_o (see Fig. 15). Due to this

repulsion, the atom S is pushed off the surface initially in state b_o^{-2}. If the holes decay before a critical distance R_c, S is recaptured; otherwise S gains sufficient kinetic energy to be desorbed. Beyond R_c, S can be neutralized leading to the desorption of neutrals (escape along b_n^{-2} where b_n is a bulk bond orbital). The maximum kinetic energy of the outgoing ions is e^2/R_o (for escape along b_o^{-2}), although the maximum ion intensity will occur at smaller energies if e.g. escape along $b_n^{-1}b_o^{-1}$ dominates. The most obvious means for decay of b_o^{-2} involves one hole hopping into the bulk without appreciable nuclear motion. However this process is blocked if U>V (V = the bond orbital interaction energy) as previously discussed in Sec. III. It may not become important until larger R values (Fig. 15) when U ≲ V. Two-hole hopping off the surface bond orbital can occur immediately, but it generally occurs with smaller probability.

To quantify the lifetime aspect of the model (90), consider a Hubbard-like single band Hamiltonian motivated through the bond-orbital approximation. Assuming that U=0 and that the bulk band is described by a Bethe lattice of half bandwidth Δ, the probability, P, of finding two holes, created in the surface bond orbital at time t=0, both in the orbital at a later time t is given by $P \sim e^{-4\alpha\Delta t/\hbar}$ if $\Delta t \ll \hbar$. The factor α ($\sim 1/2$) arises because we are considering a surface orbital. This expression must be replaced by $\beta(\hbar/\Delta t)^6$ when $\Delta t \gg \hbar$ where $\beta = 4\alpha^4/\pi^2 (1-\alpha)^8$. If $U \geq 2\Delta$ the two holes are essentially bound together

in which case $P \sim e^{-2\Delta'\alpha t/\hbar}$ so long as $\Delta' t \lesssim \hbar$ and $P_c \approx \beta^{1/2} (\hbar/\Delta' t)^3$ when $\Delta' t \gg \hbar$, where Δ' is the bound two-hole half-bandwidth. Second order perturbation theory can be used to estimate Δ'; this gives $\Delta' = 2\Delta^2/KU$, where K is the coordination number of the lattice.

The desorption or damage cross-section σ_D can be estimated from the expression (90),

$$\sigma_D(\text{theo.}) = \sum_{\text{core}} \sigma_I(\text{core})\ f_D(\text{core})\ P(t_c), \qquad (28)$$

which involves two other important factors besides $P(t_c)$ (t_c is the critical desorption time for the atom to move beyond R_c). σ_I (core) is a core ionization cross-section, which may include a back scattering factor in the solid, and can be obtained either from theory or experiment (9)). f_D is the fraction of core ionization events which result in two holes localized in a bonding orbital via the Auger process. Its magnitude can generally be determined from the Auger lineshape and indicates the importance of AES to estimating ESD cross-sections. Utilizing eq. (28), the electron beam damage cross-section of SiO_2 has been estimated to be 3×10^{-21} cm^2; experimentally it has been determined to be $\approx 2 \times 10^{-21}$ cm^2 (90). The importance of hole localization under the condition U> V can be realized from the result ($\sim 10^{-39}$ cm^2) obtained when one assumes U=0. In SiO_2, f_D for the ionization thresholds $Si_{2s,2p}$, O_{2s}, and O_{1s} have been estimated to be .13, 0, and .03 respectively (90,18). These results illustrate an important point not always fully

appreciated (84-89): each ionization or Auger yield threshold does not necessarily have a corresponding desorption threshold.

B. AES in the gas phase and chemisorbed systems

The utility of AES in the gas phase, with a reduced background and narrower Auger peaks compared to the solid phase, has been clearly demonstrated. Fig. 16 illustrates the *C KVV Auger* lineshape for some gas phase molecules. The sensitivity of AES to local hybridization (sp^3, sp^2, sp) is clearly demonstrated by the CH_4, C_2H_4, and C_2H_2 lineshapes (92,93). The insensitivity to substituent effects is demonstrated by the CH_4, CH_3OH, and $(CH_3)_2O$ (all sp^3) lineshapes. The normal alkanes (94) show a broadened sp^3 lineshape, the cyclic alkanes (95) show an apparent progression from the sp^2 to the sp^3 lineshape as the bond angle strain decreases. The constancy of the principal peak energy in the alkanes, inspite of the increasing size of the molecule, suggests the final state holes are not completely delocalized about the molecule in these systems.

The Auger lineshapes of small gas phase molecules are rather well understood. Quantitative interpretations have been reported for HF (96-98), N_2 (68), O_2 (15), CO (104,105,68), NO(68), H_2O (67,98,99), NH_3 (100-103), CH_4, C_2H_2, C_2H_4, CH_2OH (106), CO_2 (68,105), C_3O_2 (107) and SiH_4 (108) to name just some of them.

When molecules or atoms are chemisorbed on the surface of solids, the lineshape often changes little except for the

introduction of a peak or shoulder at higher electron energies as illustrated in Fig. 17. Condensation to the solid introduces the same feature as illustrated for NH_3 and H_2O. The source of this high energy feature is not well understood. At least 6 different mechanisms have been proposed; these are summarized in Table 4 along with examples and references.

The first two mechanisms listed in Table 4 may be classified as final state effects, the next two as initial state effects, the last two as chemical environment effects. In the first two mechanisms the high energy peak arises when the final state holes end up on different centers. The interatomic Auger transition model implies the intensity is determined by a two center matrix element; in the correlation model the intensity is determined by a one center matrix element. In the second and third mechanisms, the high energy peak arises because of the relaxation of the system in the presence of the initial core hole. The core hole screening mechanism implies the actual transfer of an electron into the lowest unoccupied orbital of the valence band of the adsorbate; this electron is then capable of contributing to the Auger intensity. The shake up satellite process implies the electron removed from the core is deposited into the lowest unoccupied orbital; the one hole final state relaxation processes are then significantly different to produce the high energy satellite. Finally in the last two mechanisms the high energy peaks arise from the chemical environment effects on the one electron

DOS, one mechanism concerned with the core level, the other with the valence level. In the band splitting model the chemical environment (covalent interaction) splits off a small electron density to the high energy side of the main valence peak, in the other mechanism two different chemical environments cause a "chemical" shift of the core levels which is reflected in the Auger energy.

It should not be understood that only one mechanism can be responsible for all of the high energy structure in the lineshapes for the various systems indicated in Table 4. The electron screening model as applied to CO on metals is almost certainly correct as there is other evidence, experimental (such as UPS data (128)) and theoretical (110, 129), that the electron transfer does occur. XPS and UPS data (118,119,125) also verify that band splitting may indeed occur upon chemisorption to some metals or upon covalent interaction with its neighbors. Nevertheless, in some cases the proper mechanism is not certain. As Table 4 indicates, three different mechanisms (111,121-126) have been proposed to explain the high energy structure which arises when O, C, N, or S bonds to Ni, Cu, Si, or Pt. The high energy shoulder in the O KVV spectrum of MgO and SiO_2 probably results from the same mechanism, but two different ones (114,18) have been proposed. The high energy peaks which appear in the condensed phases of H_2O and NH_3 (though not in the gas) have been explained differently (109,92,93) although they are probably due

to the same mechanism. Obviously further work is needed to determine the proper mechanism for some of these systems.

Important information on chemisorbed systems can also be obtained from the substrate Auger lineshape. Fig. 18 shows the Si $L_{23}VV$ lineshape for H (130) and O (131,132) on Si. Structure in the lineshape reveals the surface dangling bonds on clean Si, this structure decreases with exposure to either H or O indicating their use to bond the adsorbed atom. Additional features in the lineshape can also be related to the Si-H bonds or the presence of O_2 or O on Si. Very few substrate lineshapes have been reported, but these two examples indicate their usefulness in providing bonding information.

C. AES in the bulk and at interfaces

The combined surface sensitivity and DOS site specificity of AES greatly increases the utility of AES for the study of interfaces and the bulk (133). Two examples are given here. Fig. 19 shows how the Si $L_{23}VV$ lineshape changes with an increasingly thick layer of Pd deposited on the Si surface (34). With a 30 Å Pd layer on the surface, the Si lineshape is still visible. The surface sensitivity of AES indicates the Si must be diffusing into the Pd layer. Two forms of Si must exist in the Pd layer, elemental Si and Pd_2Si (34).

Fig. 19 also compares the $M_1 M_{45}V$ lineshapes of each element in the compound semiconductors GeSe (134) and GaAs (135) with UPS and XPS data. The DOS site specificity of AES is clearly

illustrated, particularly in GeSe, where each peak in the XPS spectrum can be attributed to either the Ge or Se atom. Although not quite as distinct in GaAs, the separate Auger lineshapes assist in assigning the electron density indicated by the UPS/XPS data to the separate sites. Matrix element effects and final state core hole screening effects (these are CCV lineshapes, see Sec. IV) must be included however before quantitative comparisons with the UPS/XPS data or theory (136) can be made.

Valence band information is becoming increasingly important for the study and production of new and interesting materials. These include the study of for example novel conductors (such as intercalated graphites (80,81)) semiconductors, composite materials, and ion-implanted metals. The utility of AES as a source of valence DOS information in the bulk will become more apparent as these studies continue.

VI. Summary

This review has emphasized the utilization of AES as a probe of valence electron bands and orbitals. A simple and empirical one-electron approach to the interpretation of Auger lineshapes was given to make the interpretative scheme available to a large number of experimentalists in the field. The important effects of localization and screening have been emphasized because they have been only recently identified and understood. Some areas which need further work have been indicated: they include the

local vs. Mulliken population question, the effects on the atomic matrix elements of introduction into a solid or molecule, and the sorting out of the various mechanisms proposed to interpet the appearence of high energy structure in the Auger lineshapes of small molecules and atoms chemisorbed to a surface.

A necessarily brief review and optimistic outlook for AES as a source of valence band information was given. Much information can be extracted from the Auger lineshape. However as indicated in the introduction, Auger spectra are most often utilized for elemental identification and analysis, thus ignoring this information. It is hoped this review will encourage just a few more experimentalist to utilize the information they already have at their finger tips.

VII. References

1. P. H. Holloway, Adv. in Electronics and Electron Physics 54, 241 (1980).
2. B. Crasemann, "Auger Effect and Related Topics," Lecture notes: Univ. Pierre et Marie Curie, Paris, France, 1974
3. H. Aksela, Acta Univ. Ouluensis, Ser A 89 (1980). See also J. Vayrynen, Acta Univ. Ouluensis, Ser. A 99 (1980).
4. D. E. Ramaker, J. S. Murday, and N. H. Turner, J. Electron Spect. Related Phenom. 17, 45 (1979).
5. H. N. Madden and J. E. Houston, J. Appl. Phys. 47, 3071 (1976); Solid State Commun. 21, 1081 (1977); J. Vac Sci. Technol. 14, 412 (1977).
6. F. P. Larkins, Applic. of Surf. Sci., to be published.
7. H. H. Madden, J. Vac. Sci. Technol. 18, 677 (1981).
8. W. Moddeman and K. Wittberg, "Electron Spect. Theory, Tech. and Applic." 4, ed. by C. R. Brundle and A. D. Baker (Acad. Press, N.Y., to be published).
9. G. G. Kleiman, Applic. of Suf. Sci., to be published.
10. J. C. Fuggle, "Electron Spect. Theory, Tech. and Applic." 4, ed. by C. R. Brundle and A. D. Baker (Acad. Press, N.Y., to be published).
11. M. O. Krause, J. Phys. Chem. Ref. Date 8, 307 (1979).
12. J. S. Murday, "Review of Surface Physics," NRL Memorandum Report 3062, May 1975; See also C. C. Chang, J. Vac. Sci. Technol. 18, 276 (1981).
13. J. W. Mayer and A. Turos, Thin Solid Films 19, 1 (1973); C. A. Evan in NBS Special Public. 400-23, March 1976.
14. D. E. Ramaker, J. S. Murday, N. H. Turner, G. Moore, M. G. Lagally, and J. Houston, Phys. Rev. B19, 5375 (1979).
15. B. I. Dunlap, P. A. Mills, and D. E. Ramaker, J. Chem Phys. 75, 300 (1981).
16. D. A. Shirley, Chem. Phys. Letters, 17, 312 (1972); 16, 220 (1972); Phys Rev. A 7, 1520 (1973).
17. J. B. Mann, Los Alamos Scientific Laboratory Report No LASL-3690, 1967 (unpublished).
18. D. E. Ramaker, Phys. Rev. B21, 4608 (1980).
19. E. J. McGuire, Phys Rev. 185, 1 (1969); 2 273 (1970).
20. E. J. McGuire, Phys Rev. A3, 1801 (1971).
21. D. L. Walters and C. P. Bhalla, Phys Rev. A3, 1919 (1971); Atomic Data 3, 301 (1971).
22. D. L. Walters and C. P. Bhalla, Phys. Rev. A4, 2164 (1971).
23. D. E. Ramaker, submitted for publication in Chem Phys lett.
24. E. J. McGuire, Sandia Laboratories Reserach Report SC-RR-69-137, June 1969.
25. M. H. Chen and B. Crasemann, Phys. Rev. A8, 7 (1973)
26. M. H. Chen and B. Crasemann, Phys. Rev. A16, 1495 (1977).
27. J. Vayryen, J. Elect. Spect. Related Phenom. 22, 27 (1981).
28. C. P. Bhalla, N. O. Folland, and M. A. Hein, Phys. Rev. A8, 649 (1973)

29. E. J. McGuire, Phys. Rev. A16, 2365 (1977).

30. F. L. Hutson, D. E. Ramaker, and B. I. Dunlap, J. D. Ganjei, and J. S. Murday, to be published in J. Chem Phys.

31. J. A. D. Matthews and Y. Komninos, Surf. Sci 53, 716 (1975).

32. D. R. Jennison, Phys. Rev. Letters 40, 807 (1978).

33. S. D. Bader, L. Richter, and M. B. Brodsky, Solid State Commun. 37, 729 (1981).

34. G. W. Rubloff, P. S. Ho, J. F. Freeouf, and J. E. Lewis, Phys. Rev. B23, 4183 (1981); P. S. Ho, G. W. Rubloff, J. E. Lewis, V. L. Moruzzi, and A. R. Williams, Proc. Electrochem. Soc. 80,, 85 (1980).

35. M. Cini, Solid State Commun 20, 605 (1976); Phys. Rev. B17, 2788 (1978). G. A. Sawatzky, Phys. Rev. Lett. 39, 504 (1977).

36. M. Cini, Phys. Rev. 87, 483 (1979); G. Treglia, M. C. Desjonqueres, F. Ducastelle, and D. Spanjaard, to be publ. in J. Phys. C.; P. T. Andrews, T. Collins, and P. Weightman, to to publ. in J. Phys. C.

37. B. I. Dunlap, F. L. Hutson, and D. E. Ramaker, J. Vac. Sci. Technol. 18, 556 (1981).

38. P. Weightman and P. T. Andrews, J. Phys. C 12, 943 (1979).

39. H. H. Madden, D. M. Zehner, and J. R. Noonan, Phys. Rev. B17, 3074 (1978).

40. E. Antonides, E. C. Janse, and G. A. Sawatky, Phys. Rev. B15, 1669 (1977); E. Antonides and G. A. Sawatzky, Inst. Phys. Conf. Ser. No. 39, 134 (1978).

41. F. J. Himpsel, P. Heimann, and D. E. Eastman, J. Appl. Phys. 52, 1658 (1981).

42. P. J. Bassett, T. E. Gallon, J. A. D. Matthew, and M. Prutton, Surf. Sci. 35, 63 (1973).

43. J. M. Burkstrand and Tibbetts, Phys. Rev. 15, 5481 (1977).

44. J. M. Mariot and G. Dufour, J. Elect. Spect. Related Phenom. 13, 403 (1978).

45. A. C. Parry-Jones, P. Weightman, and P. T. Andrews, J. Phys. C12, 1587 (1979).

46. J. A. D. Matthew, J. Phys. C11, L47 (1978).

47. C. J. Powell, Solid State Commun. 26, 557 (1978).

48. L. Oberli, R. Monot, H. J. Mathieu, D. Landolt, and J. Buttet, Surf. Sci. 106, 301 (1981).

49. T. Jach and C. J. Powell, Phys. Rev. letters, 46, 953 (1981).

50. P. Weightman and P. T. Andrews, J. Phys. C13, L815 (1980).

51. G. A. Sawatzky and D. Post, Phys. Rev. B20, 1546 (1979).

52. S. P. Withrow, P. E. Luscher, F. M. Propst, and W. H. Weinberg, J. Vac. Sci. Technol. 15, 511 (1978).

53. J. F. McGilp, P. Weightman, and E. J. McGuire, J. Phys. C10, 3445 (1977).

54. A. C. Parry-Jones, P. Weightman, and P. T. Andrews, J. Phys. F5, 590 (1975).

55. W. A. Harrison, "Electronic Structure and the Properties of Solids" (W. H. Freeman & Co., San Francisco, 1980), p.476.

56. J. S. Murday, D. E. Ramaker, N. K. Bernett, and N. H. Turner, Proc. Int. Vac. Congr. 7th 2, 1293 (1977).

57. D. E. Ramaker and J. S. Murday, J. Vac. Sci. and Technol. 16, 510 (1979).

58. D. R. Jennison, J. Vac. Sci. Technol. 18, 466 (1981); Bull. Am. Phys. Soc. 26, 220 (1981).

59. G. A. Sawatzky and A. Lenselink, Phys. Rev. B21, 1790 (1980).

60. O. Gunnarsson and K. Schonhammer, Phys. Rev. B22, 3710 (1980).

61. D. E. Ramaker, submitted to Phys. Rev. B.

62. W. Domcke, L. S. Cedarbaum, J. Schirmer, and W. von Niessen, *Phys. Rev. Letters* 42, 1237 (1979); Chemical Phys 39, 149 (1979).

63. T. A. Carlson and C. W. Nestor, Jr., Phys. Rev. A8, 2887 (1973).

64. H. Korber, and W. Mehlhorn, Z. Physik 191, 217 (1965); W. Mehlhorn, D. Stalherm, and H. Verbeek, Z. Naturforsch 23A, 287 (1968).

65. M. O. Krause, T. A. Carlson, and W. E. Moddeman, J. Phys. Coll. C4 32, 139 (1971); M. O. Krause, F. A. Stevie, L. J. Lewis, T. A. Carlson, and W. E. Moddeman, Phys. Lett 31A, 81 (1970).

66. W. E. Moddeman, T. A. Carlson, M. O. Krause, B. P. Pullen, W. E. Bull, and G. K. Schweitzer, J. Chem Phys. 55, 2317 (1971).

67. H. Agren and H. Siegbahn, Chem. Phys. Letters 69, 424 (1980).

68. H. Agren, J. Chem Phys. 75, 1267 (1981); J. Muller, H. Agren, O. Goscinski, Chem. Phys Lett. 38, 349 (1979).

69. J. N. Schulman and J. D. Dow, Phys. Rev. Letters 47, 371 (1981).

70. G. van der Laan, C. Westra, C. Haas, and G. A. Sawatzky, Phys. Rev. B23, 4369 (1981).

71. U. von Barth and G. Grossman, Solid State Commun. 32, 645 (1979); Physica Scripta 21, 580 (1980).

72. G. D. Mahan, Phys. Rev. B21, 1421 (1980).

73. L. C. Davis and L. A. Feldkamp, Phys. Rev. B23, 4269 (1981).

74. V. I. Grebennikov, Y. A. Babanov, and O. B. Sokolov, Phys. Stat. Sol. 80, 73 (1977).

75. R. Lasser and J. C. Fuggle, Phys. Rev. B22, 2637 (1980).

76. N. D. Lang and A. R. Williams, Phys. Rev. B16, 2408 (1977); 20, 1369 (1979); A. R. Williams and N. D. Lang, Phys. Rev. Letters 40, 954 (1978).

77. D. R. Jennison, Phys. Rev. A23, 1215 (1981).

78. D. R. Jennison, H. H. Madden, and D. M. Zehner, Phys. Rev. B21, 430 (1980).

79. D. R. Jennison, Phys. Rev. B18, 6996 (1978).

80. J. S. Murday, B. I. Dunlap, F. L. Hutson, II, and P. Oelhafen, to be published in Phys. Rev. B.

81. B. I. Dunlap, D. E. Ramaker, and J. S. Murday, Submitted to Phys. Rev. B.

82. J. H. O. Varley, J. Phys. Chem. Solids 23, 985 (1962).

83. M. L. Knotek and P. J. Feibelman, Phys. Rev. Letter 40, 964 (1978); Suf. Sci. 90, 78 (1979); Phys. Rev. B18, 653 (1978); P. J. Feibelman, Surf. Sci. 102, L51 (1981).

84. T. E. Madey, R. Stockbauer, S. A. Flodstrom, J. F. van der Veen, F. J. Himpsel, and D. E. Eastman, Phys. Rev. B23, 6847 (1981).

85. G. G. Pantano and T. E. Madey, Appl. of Surf. Sci. 7, 115 (1981)

86. F. P. Netzer and T. E. Madey, Submitted to J. Chem. Phys.

87. R. Franchy and D. Menzel, Phys. Rev. Letters 43, 865 (1979).

88. P. Feulner, R. Treichler, and D. Menzel, Submitted to Phys. Rev. B (Rapid Commun.)

89. R. Jaeger, J. Stohr, J. Feldhaus, S. Brennan, and D. Menzel, Phys. Rev. B23, 2102 (1981).

90. D. E. Ramaker, C. T. White, and J. S. Murday, J. Vac. Sci. Technol. 18, 748 (1981); also submitted to Phys. Letters.

91. E. J. McGuire, Phys. Rev. A16, 73 (1977); J. I. Vrakking and F. Meyer, Surf. Sci. 47, 50 (1975).

92. R. R. Rye, T. E. Madey, J. E. Houston, and P. H. Holloway, J. Chem. Phys. 69, 1504 (1978).

93. R. R. Rye, J. E. Houston, D. R. Jennison, T. E. Madey, and P. H. Holloway, Ind. Eng. Chem. Prod. Res. Dev. 18, 1 (1979).

94. R. R. Rye, D. R. Jennison, and J. E. Houston, J. Chem. Phys. 73, 4867 (1980).

95. J. E. Houston and R. R. Rye, J. Chem. Phys. 74, 71 (1981).

96. K. Faegri, Jr., and H. P. Kelly, Phys. Rev. A19, 1649 (1979); O. M. Kvalheim and K. Faegri, Chem. Phys. Letters 67, 127 (1979).

97. R. W. Shaw, Jr., and T. D. Thomas, Phys. Rev. A11, 1491 (1975).

98. I. H. Hillier and J. Kendrick, Mole. Phys. 31, 849 (1976).

99. H. Agren, S. Svensson, and U. I. Wahlgren, Chem. Phys. Letters, 35, 330 (1975).

100. J. M. White, R. R. Rye, and J. E. Houston, Chem. Phys. Lett. 46, 146 (1977).

101. R. W. Shaw, Jr., J. S. Jen, and T. D. Thomas, J. Electron Spect. Related Phenom. 11, 91 (1977).

102. F. P. Larkins and A. Lubenfeld, J. Electron Spect. Related Phenom. 15, 137 (1979).

103. M. T. Okland, K. Faegri, and R. Manne, Chem. Phys. Letters 40, 185 (1976).

104. H. Agren and H. Siegbahn, Chem. Phys. Letters 72, 498 (1980).

105. D. R. Jennison, J. A. Kelber, and R. R. Rye, Chem. Phys. Letters 77, 604 (1981); J. A. Kelber, D. R. Jennison and R. R. Rye, J. Chem. Phys. 75, 652 (1981).

106. D. R. Jennison, Chem. Phys. Letters 69, 435 (1980).

107. L. Karlson, L. O. Werme, T. Bergmark, and K. Siegbahn, J. Elect. Spec. Related Phenom. 3, 181 (1974).

108. F. Maracci, R. Platania, and R. Salomone, J. Electron Spect. Related Phenom. 19, 155 (1980).

109. C. T. Campbell, J. W. Rogers, Jr., R. L. Hance, and J. M. White, Chem. Phys. Lett. 69, 430 (1980).

110. D. R. Jennison, G. D. Stucky, R. R. Rye, and J. A. Kelber, Phys. Rev. Lett. 46, 911 (1981).

111. M. Salmeron, A. M. Baro, and J. M. Rojo, Phys. Rev. B13, 4348 (1976).

112. P. H. Citrin, J. E. Rowe, and S. B. Christman, Phys. Rev. B14, 2642 (1976).

113. T. E. Gallon and J. A. D. Matthew, Phys. Status Solidi 41, 343 (1970).

114. P. J. Bassett, T. E. Gallon, J. A. D. Matthew, and M. Prutton, Surf. Sci. 35, 63 (1973).

115. E. W. Plummer, W. R. Selanck, and J. S. Miller, Phys. Rev. B18, 1673 (1978).

116. F. P. Netzer and J. A. D. Matthew, J. Electron Spectros. Related Phenom. 16, 359 (1979).

117. J. C. Fuggle and D. Menzel, Surf Sci. 79, 1 (1979).

118. L. A. Harusak and L. L. Tongson, J. Appl. Phys. 50, 4350 (1979).

119. M. A. Smith and L. L. Levenson, Phys. Rev. B16, 1365 (1977).

120. A. Hiraki, S. Kim, W. Kammura, and M. Iwami, Appl. Phys. Lett. 34, 194 (1979).

121. J. P. Coad and J. C. Riviere, Proc. R. Soc. Lond. A331, 403 (1972).

122. K. Kinimori, T. Kawai, T. Kondow, T. Onishi, and K. Tamaru, Surf. Sci. 46, 567 (1974).

123. E. N. Sickafus and F. Steinrisser, J. Vac. Sci. Technol. 10, 43 (1973).

124. E. N. Sickafus, Phys. Rev. B7, 5100 (1973).

125. G. G. Tibbetts, J. M. Burkstrand, and J. C. Tracy, Phys. Rev. B15, 3652 (1979).

126. W. Losch, J. Vac. Sci. Technol. 16, 865 (1979).

127. P. Legare, G. Maire, B. Carriere, and J. P. Deville, Surf. Sci. 68, 348 (1977).

128. C. F. Bruckner and T. N. Rhodin, Surf. Sci. 86, 638 (1979).

129. K. Hermann and P. S. Bagus, Phys. Rev. B16, 4195 (1977).

130. H. H. Madden, Surf. Sci. 105, 129 (1981).

131. M. C. Munoz, V. Martinez, J. A. Tagle, and J. L. Sacedon, Phys. Rev. Lett. 44, 814 (1980).

132. B. Lang, P. Scholler, and B. Carriere, Surf. Sci. 99, 103 (1980).

133. J. A. Tagle, V. M. Saez, J. M. Rojo, and M. Salmeron, Surf. Sci. 79, 77 (1978).

134. G. D. Davis, P. E. Viljoen, and M. G. Lagally, J. Elect. Spec. Related Phenom. 21, 135 (1980).

135. G. D. Davis and M. G. Lagally, J. Vac. Sci. Techol. 15, 1311 (1978); G. D. Davis, D. E. Savage, M. G. Lagally, J. Electron. Spectrosc. Related Phenom. 23, 25 (1981).

136. G. De Meyer, R. Hoogewijs, W. Lambrecht, J. Vennik, and G. Dalmai, Surf. Sci. 106, 498 (1981).

TABLE I. RECENT AES REVIEW ARTICLES

	Author	Principle topics covered
1.	Holloway (1) (1980)	Experimental approach and applications Extracting the lineshape from exp. data
2.	Larkins (6) (1981)	Auger energies - chemical shifts and solid state shifts Energies of Auger satellites
3.	Madden (7) (1981)	Chemical info. from AES - chemical shifts and lineshapes Applications to insulators and metals
4.	Moddeman (8) (1981)	Auger effect in atoms and molecules Gas phase experiments
5.	Aksela (3) (1981)	Auger lineshapes of transition metals in the gas phase Lineshape interpretation in the atomic model
6.	Crasemann (2) (Unpub.)	Auger effect in atoms Matrix elements, angular momentum coupling, Auger widths and fluorescecence yields
7.	Kleiman (9) (1981)	Effects of localization and screening on Auger energies Applications to d band metals and alloys
8.	Fuggle (10) (1981)	Screening and localization effects on the Auger lineshape Applications to metals and insulators
9.	This work	Auger as a probe of valence bands - radial extent, localization, and screening effects on lineshape Applications to metals, insulators, molecules

TABLE 3 - COMPARISON OF ACTUAL AUGER INTENSITIES WITH THOSE OBTAINED FROM INITIAL AND FINAL STATE POPULATIONS.

	$\pi_u^{-1} 2\sigma_u^{-1}$	$\pi_u^{-1}(\pi_u, 3\sigma_g)^{-1}$	$\pi_g^{-1}(\pi_u, 3\sigma_g)^{-1}$
O_2 O KVV (15)			
X_i initial state	2.0	6	1.6
X_f final state	1.9	6	2.8
Exp.	2.3	6	4
	$1e_g^{-2}$	$1e_u^{-1} 1e_g^{-1}$	$1e_g^{-2}$
C_2H_6 C KVV (77)			
RHF-SCF initial state	68	16	1
RHF-SCF final state	.9	1.9	1
Full theo. matrix element	1.2	3.0	1
	$2e^{-2}$	$2e^{-1}(4e, 3\pi, 1a_2)^{-1}$	$(4e, 3\pi, 1a_1)^{-2}$
NO_3 N KVV (30,61)			
X_i initial state	1	7.4	13
X_f final state	1	5	2.5
Empirical fit to data	≈ 1	≈ 5	≈ 2.5

TABLE 2

Comparison of PES, XES, and AES Features (12,13)

Method	Probe Input	Measurement Output	Minimum Probe Diameter (um)	Sampling Depth Atomic Layers	Optimum Detection Sensitivity (ppm atomic)	Sampling Region of Valance Density of States
Electron Excited XES	Monoenergetic electrons 10-3000 ev	X-rays 10-1500 ev	.5-100	10^4	1-100	Site specific
Photon Excited XES	X-ray beam ~1.5 kev	X-rays 10-1500 ev	10^4	10^5	1-100	Site specific
Electron Excited AES	Monoenergetic electrons 10-3000 ev	Electrons 10-1500 ev	.5-100	2-10	10^3-10^4	Site specific
Photon Excited AES	X-ray beam ~1.5 kev	Electrons 10-1500 ev	10^4	2-10	10^3-10^4	Site specific
PES*	Monoenergetic photon beam	Electrons 0-1500 ev	10^4	2-100	10^4	All sites

*PES here includes both x-ray and ultraviolet photoelectron spectroscopy (XPS and UPS)

TABLE 4 - SUMMARY OF MECHANISMS RECENTLY PROPOSED FOR THE EXISTENCE OF HIGH ENERGY STRUCTURE ABOVE THE PRINCIPLE AUGER PEAK.

Suggested mechanism	Example	Reference[a]
1) Interatomic Auger transition	MgF_2, NaF	Citrin (112)
	LiF	Gallon & Matthew (113)
	MgO	Bassett (114)
	S, C, O, N on Ni, Cu, Fe	Salmeron & Baro (111)
2) Final state hole-hole correlation effects	Cu	Madden (39)
	Cu, Ni, Zn	Antonides (40)
	SiO_2	Ramaker (18)
3) Electron transfer or core hole screening	$Cr(CO)_6$, $W(CO)_6$	Plummer (116), Jennison (110)
	CO on Pt, Ru, N_2 on W	Netzer & Matthew (116)
		Huggle & Menzel (117)
4) Shake satellites	Condensed NH_3	Larkins & Lubenfeld (102)
	NH_3 on Al, Al_2O_3	Campbell (139)
5) Band splitting due to covalent interaction with substrate or other atoms.	FeS_x	Marusak & Tongson[b] (118)
	TiC, VC, Cr_3C_2	Smith & Levenson (119)
	condensed H_2O	Rye (92,93)
	Al, Si, P, S dissolved in Cu	Hiraki (120)
	O, S, on Ni, Mo, Si, Cu	Coad & Riviere (121), Kunimori (122), Sickafus (123,124), Tibbetts (125)
	C_2H_4, C_2H_2, C_2N_2 On Pt	Netzer & Matthew (116)
6) Two different chemical environments present; shift of core level	S on Cu-Au alloy	Losch (126)
	O_2 on Si, Pt	Legare (127)
	Pt, Sn on Al_2O_3	Legare (127)

[a] If more than two authors, only the first is listed.

[b] Indicated inter-atomic Auger transition also possible.

Figure Captions

Fig. 1 An illustration of photoemission, (XPS), x-ray emission (XES), and Auger emission (AES) in an atom involving the K and L levels. The shake-off process with a subsequent Auger emission yielding a KL-LLL shake/Auger satellite is also illustrated. Filled circles represent electrons, open circles holes in the K and L shells.

Fig. 2 Comparison of the KLL theoretical and experimental atomic Auger matrix elements $P_{c\underline{ll}'}$ for atoms in the first two rows of the periodic table as given in ref. (23). Z is the nuclear charge, $P_{c\underline{ll}'}$ is the matrix element per filled shell as indicated by eqs. (9) and (10). $P_{c\underline{ll}'}$ has been normalized for each atom such that P_{cpp} is 100. The theoretical data of McGuire (19, McG) has been scaled by factors f_{ss} =.65 and f_{sp}=.81, that of Walters and Bhalla (21, W & B), by factors f_{ss}=.59 and f_{sp}=.78 to correspond to the experimental data for Ne (Z=10). The data of Chen and Craemann (25, C & C) is unscaled. Sources for the experimental points are given in Ref. 23. Results of a one-electron hole calculation for Ne (28) are indicated by the solid squares. The brackets indicate stated uncertainties, arrows indefinite estimated uncertainties in experimental data.

Fig. 3 Comparison of the $L_{23}VV$ theoretical and experimental atomic Auger matrix elements $P_{c\underline{\alpha}\underline{\alpha}'}$ for atoms in the 2nd and 3rd rows of the periodic table as given in ref. 23. $P_{c\underline{\alpha}\underline{\alpha}'}$ is defined and normalized as in Fig. 1. The theoretical data of McGuire (20) has been scaled by factors f_{ss}=1.97, f_{sp}=1.23, f_{sd}=1.33, f_{pd}=1.27 and f_{dd}=2.06, that of Walters and Bhalla (22) by f_{ss}=1.94, f_{sp}=1.03, f_{sd}=1.32, f_{pd}=1.24, and f_{dd}=2.05, to correspond to the Ar (Z=18) ss and sp and the Kr(Z=36) sd, pd, and dd experimental data. The data of Chen and Crasemann (26) is unscaled. Sources of the experimental data may be obtained from ref. 23. The crossed symbols for Z=18 and 36 refer to earlier experimental data, for Z=29 to a CI calculation for Cu (29).

Fig. 4 Comparison of Γ_{nd} with U^e_{ndnd} for the metals with electron configuration d^6s^2 to $d^{10}s^2p^2$. The 3d and 4d data is from refs. 40, 41, 54 and 47, U^e_{5d5d} from refs. 47 and 53, Γ_{5d} calculated or obtained from refs. 47 and 55. Metals with band like and atomic like lineshapes are indicated, those between the dashed lines are "transitional."

Fig. 5 Comparison of the core-(valence d)-(valence d) Auger lineshapes for the 'transitional' metals as indicated in Fig. 4 with the fold of the one-electron DOS, N(E).

Data for Cu, Ag, and Au from Powell (47), for Ni and Pd from Kleiman (9). The vertical bars for Cu and Ag indicate results from an atomic calculation (38, 45). E_x is the core binding energy, E_A the Auger electron energy.

Fig. 6 Comparison of the effective hole-hole repulsion, U^e_{xx}, $U^e_{\underline{\alpha}\underline{\alpha}}$, or U^e_{vv}, with the corresponding interaction parameter, V, γ, or Γ for NO_3^-, $SO_4^{=}$, and SiO_2 (37). The definition of each parameter is illustrated on the left for NO_3^-. AO, LO, MO refer to atomic, lobe, or molecular orbitals, also illustrated. $U^e_{\underline{\alpha}\underline{\alpha}\underline{\alpha}}$ is the effective 3 hole lobe orbital repulsion energy (37).

Fig. 7 Top) Comparison of the experimental and total theoretical N KVV lineshapes for $NaNO_3$ as obtained utilizing a two and three hole final state described by a NO_3^- MO (30).

Middle) The parent Auger and shake/Auger contributions compared to the experimental lineshape.

Bottom) Comparison of the theoretical shake lineshape with the difference between the experimental and theoretical parent Auger lineshapes.

Fig. 8 Same as Fig. 7 for Li_2SO_4 except the ΔE between the shake/Auger and parent Auger lineshapes, eq. (22), was reduced to -2eV indicating the preferred 2 hole $SO_4^{=}$ MO and 3 hole S-O LO final state description. Data from refs. 37 and 56.

Fig. 9 a) Comparison of the experimental (solid) and theoretical (dotted) O KLL lineshapes for SiO_2 as obtained utilizing a Si-O-Si LO (57, 14, 37).

b) The difference between the experimental and theoretical lineshapes. The peaks at 475 and 495eV have been attributed to shake/Auger satellites, the peak at 510 eV to delocalization (18).

c) Comparison of the experimental (solid) and theoretical (dotted) Si $L_{23}VV$ lineshapes as obtained utilizing a SiO_4^{4-} MO (57, 14, 37). The vertical bars indicate results of a cluster CI calculation (18), the dotted bars denoting Si-O-Si localized holes, the solid bars delocalized holes.

d) The difference between the experimental and theoretical lineshapes. The peaks at 55 and 68eV may be attributed to the localized hole contributions, that at 84 eV to beam damage (18).

Fig. 10 Lower left: the percent non-local intensity of the total versus U/Γ. U is the one center hole-hole repulsion, Γ the band width, and $U^e \approx U-U_{ij}$ is an effective Coulomb repulsion.

Upper right: the difference in energy between the centroids of the local and non-local Auger contributions. ΔE_o is the shift in energy of the local contribution from the initial band center. The diagonals

E-U and U^e are also indicated. The results obtained from a 16 atom cluster in a tetrahedral lattice (18) with $U_{ij}= 0$ and $U_{ij} \neq 0$ (U_{ij} is the two center Coulomb repulsion energy) are compared with the results of Sawatzky and Lenselink (59) for an infinite simple cubic lattice with $U_{ij} = 0$.

Fig. 11 Comparison of the experimental N KVV lineshape for $LiNO_3$ with that calculated utilizing an $X\alpha$ theoretical local DOS from the initial (core hole) and final (no core hole) state wavefunctions (30, 61).

Fig. 12 Top) Comparison of the experimental Be KVV Auger lineshape with that calculated utilizing a HF-SCF local DOS from the final state (77).

Bottom) Same as the top except the relative ss, sp, and pp areas are determined by the initial state. Complete s electron screening is assumed in the initial state (75).

Fig. 13 Top) The Cu M_1VV experimental Auger spectrum as reported in ref. (78). The narrow localized d^2 contribution is indicated by the dotted line, the difference represents the bandlike sd contribution.

Bottom) Comparison of the sd Auger contribution as obtained above (solid) with the calculated Auger lineshape (dotted). The calculated lineshape is obtained from the final DOS but with the relative sd/dd area increased by

a factor of 2 consistent with the $d^{10}s^2$ initial state configuration. Complete s electron screening is again assumed in the initial state (78, 75).

Fig. 14 Comparison of the DOS as determined in ref. (80) from a quantitative interpretation of the C KVV Auger lineshape (solid) with UPS data (dotted) for the intercalated graphite systems C_8Cs and C_6Li.

Fig. 15 Schematic potential energy curves (90) for interaction between a bulk atom B and a surface atom S, before (lower ground state curve) and after the Auger process. Curves are labeled by the bond orbital hole states and by the separated state of the surface atom. B' denotes bulk atoms not bonded to S, E_b and E_s are the bulk and surface atom ionization potentials, E_B and U are the bond orbital binding energy and hole-hole repulsion energy.

Fig. 16 The C KVV Auger lineshapes taken in the gas phase for various carbon molecules illustrating the sensitivity to sp^n hydrization (92-95).

Fig. 17 Comparison of some KVV lineshapes of molecules in the gas phase with those in the chemisorbed, condensed, or metal ligand state illustrating the appearance of structure at higher energies. The NH_3 data is taken from ref. 109, CO data from ref. 110, O/Cu data from ref. 111, and H_2O data from refs. 92, 93. E_A is the Auger

energy, E_K the O 1s binding energy. All spectra are N(E) except for O/Cu.

Fig. 18 The substrate Si $L_{23}VV$ Auger data for either H/Si (130), left, or O/Si (131), right.
H/Si) Comparison of the theoretical and experimental difference spectra (H/Si-clean Si) with the spectrum from gas phase SiH_4. Region A shows the decrease in surface dangling bond states, peaks B and C arise from Si-H bonds as indicated by the SiH_4 spectrum (130)
O/Si) Comparison of the Auger transition DOS (self deconvolution of the Auger lineshape) for clean Si and O/Si. Region A shows the decrease in surface dangling bonds, structure in region B corresponds to O_2 molecular orbitals on Si, structure in region C to O-Si bonds (131). E_A is the Auger energy, E_B the binding energy.

Fig. 19 Top) Comparison of the Si $L_{23}VV$ Auger lineshape with coverage of Pd as indicated in Angstroms (Å) (34).
Bottom) Comparison of the $M_1M_{45}V$ Auger lineshapes with XPS and UPS data for GeSe (134) and GaAs (135). The $M_1M_{45}V$ sum for GaAs corresponds to a direct sum of the Ga and As $M_1M_{45}V$ lineshapes. E_A is the Auger energy, E_B the binding energy.

SHAKE-OFF XPS

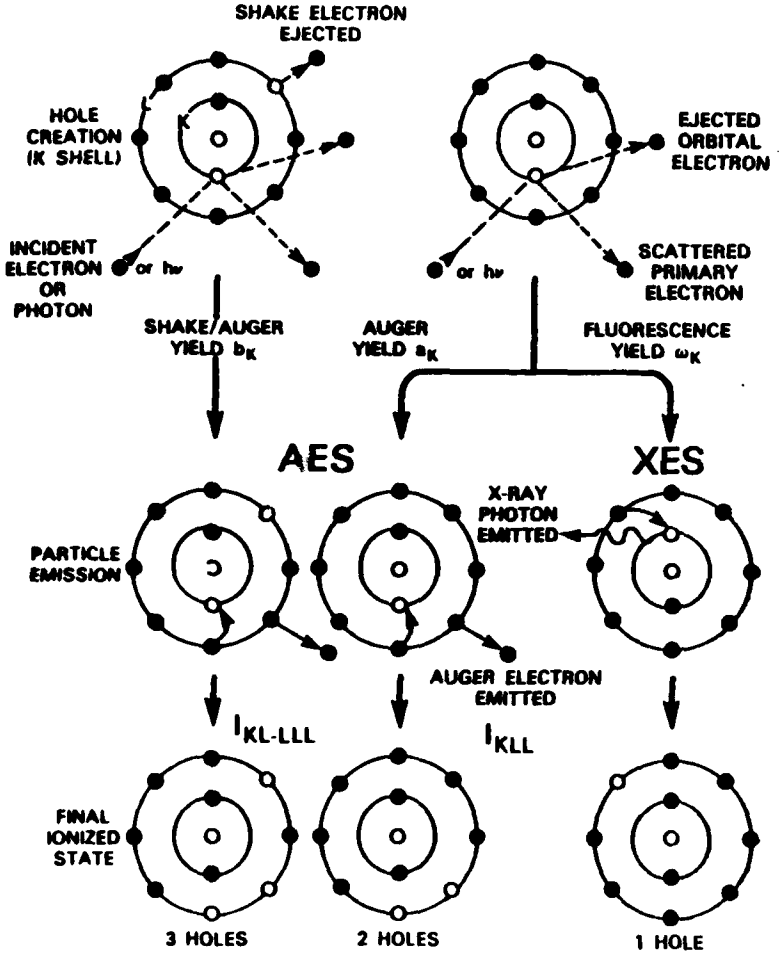

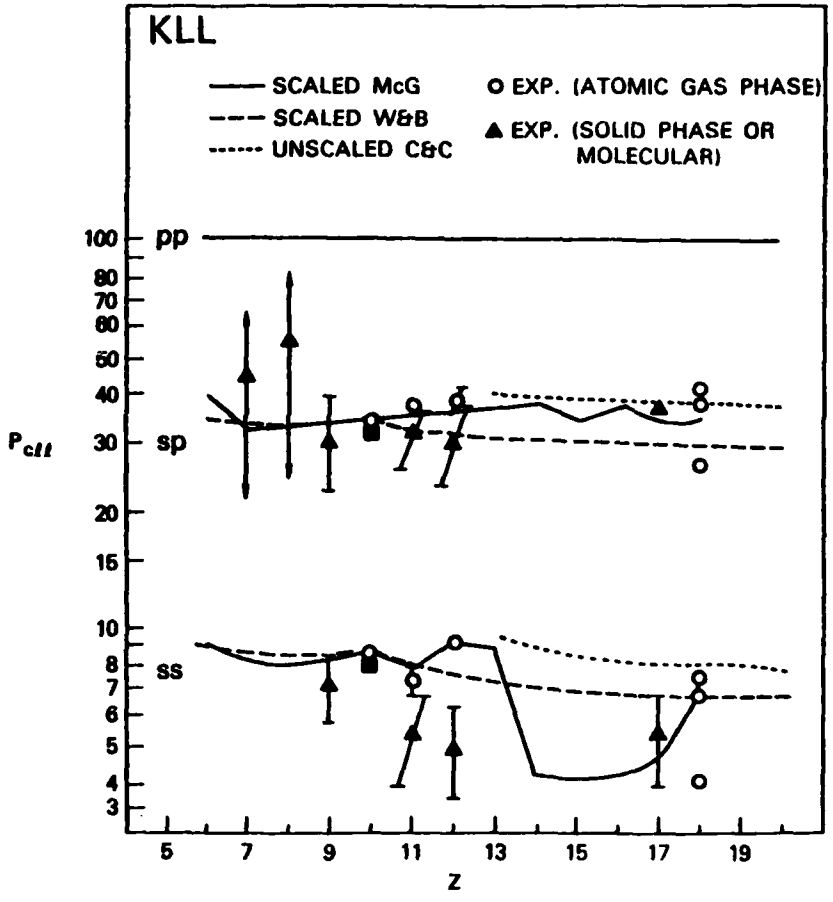

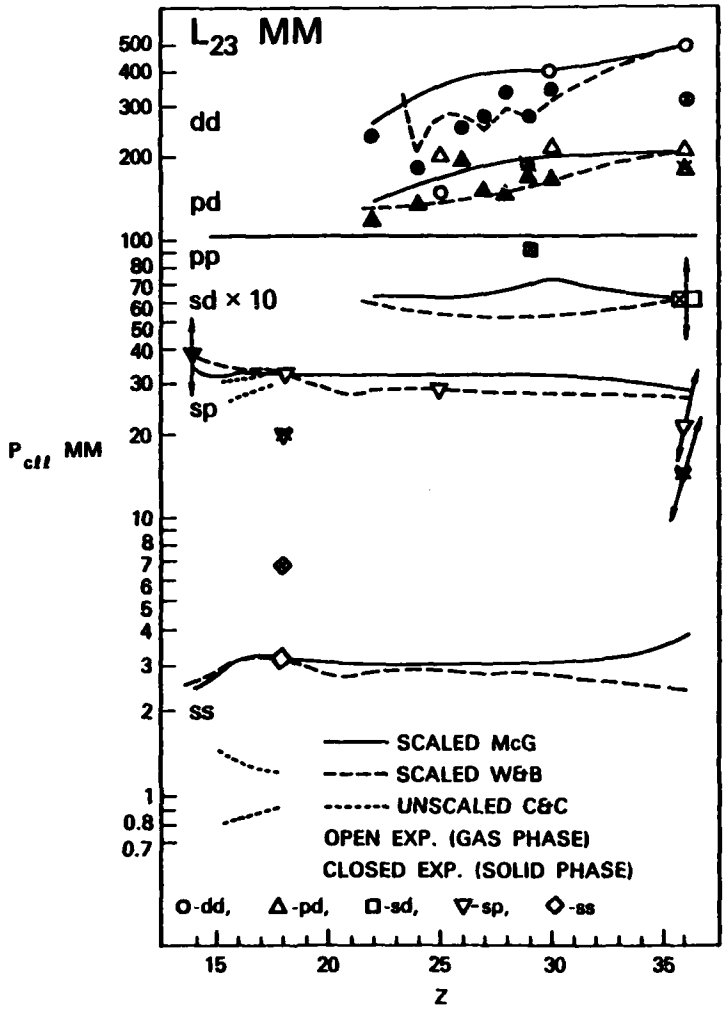
L23 MM
dd
pd
pp
sd × 10
sp
ss
P cll MM
SCALED McG
SCALED W&B
UNSCALED C&C
OPEN EXP. (GAS PHASE)
CLOSED EXP. (SOLID PHASE)
O-dd, Δ-pd, □-sd, ▽-sp, ◇-ss
Z

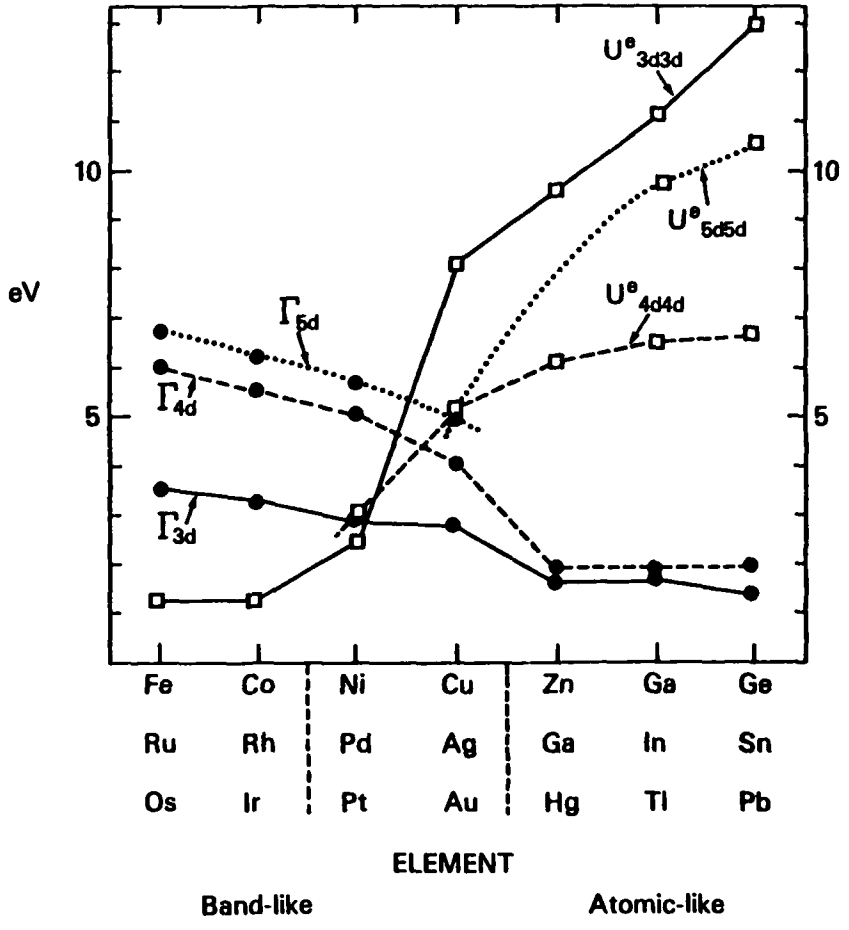
eV
10
5
U e 3d3d
U e 5d5d
U e 4d4d
Γ 5d
Γ 4d
Γ 3d
Fe Co Ni Cu Zn Ga Ge
Ru Rh Pd Ag Ga In Sn
Os Ir Pt Au Hg Tl Pb
ELEMENT
Band-like
Atomic-like

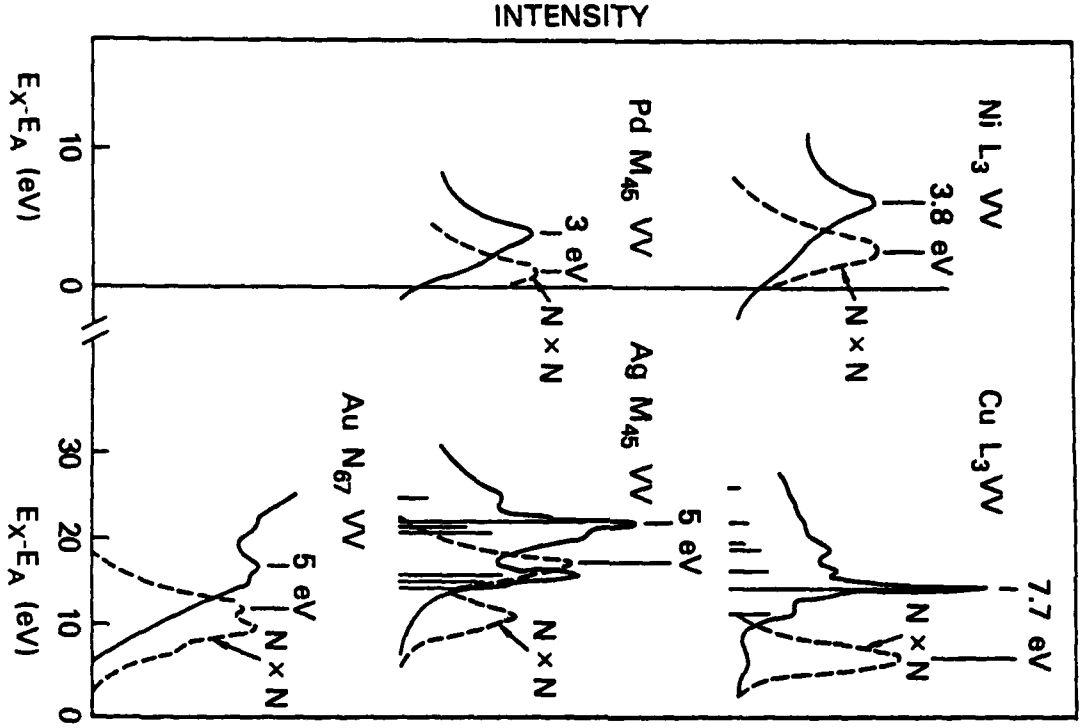
INTENSITY
E_X-E_A (eV)
Ni L_3 VV
3.8 eV
N x N
Pd M_{45} VV
3 eV
N x N
Cu L_3VV
7.7 eV
N x N
Ag M_{45} VV
5 eV
N x N
Au N_{67} VV
5 eV
N x N

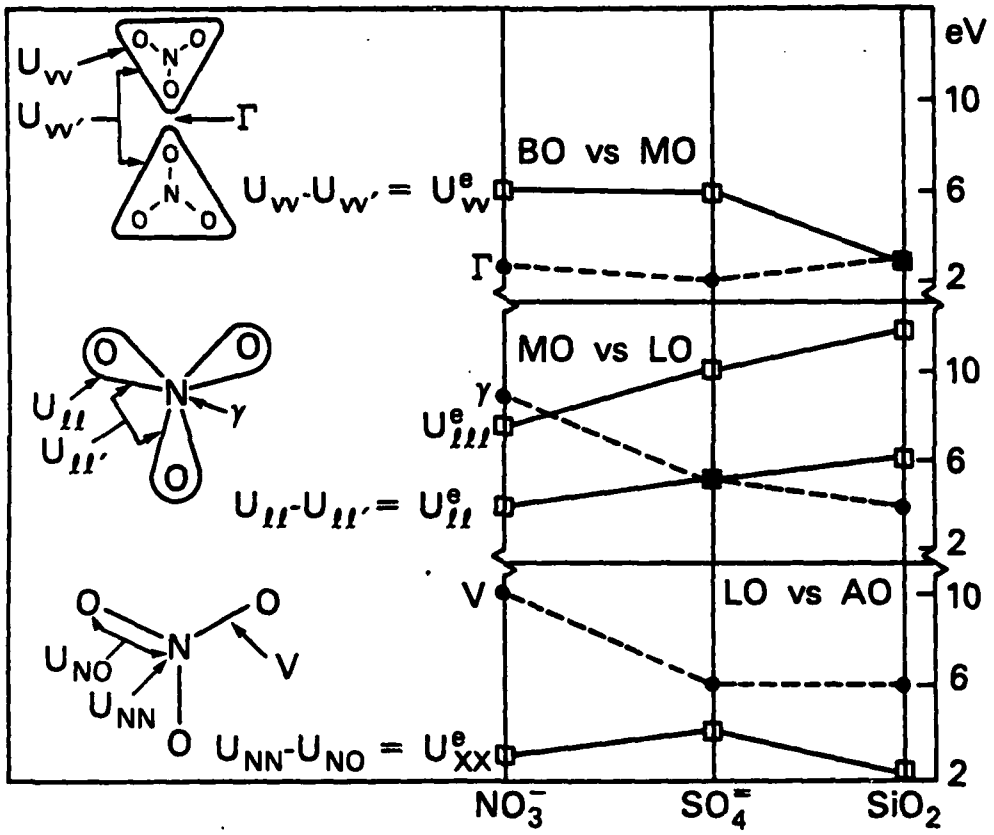
U_{WW}
$U_{WW'}$
Γ
$U_{WW'} = U^e_W$
BO vs MO
U_{ll}
$U_{ll'}$
γ
$U_{ll'} = U^e_{ll}$
MO vs LO
U_{NO}
U_{NN}
V
U_{NN}-U_{NO} = U^e_{XX}
LO vs AO
eV
10
6
2
NO_3^-
$SO_4^=$
SiO_2

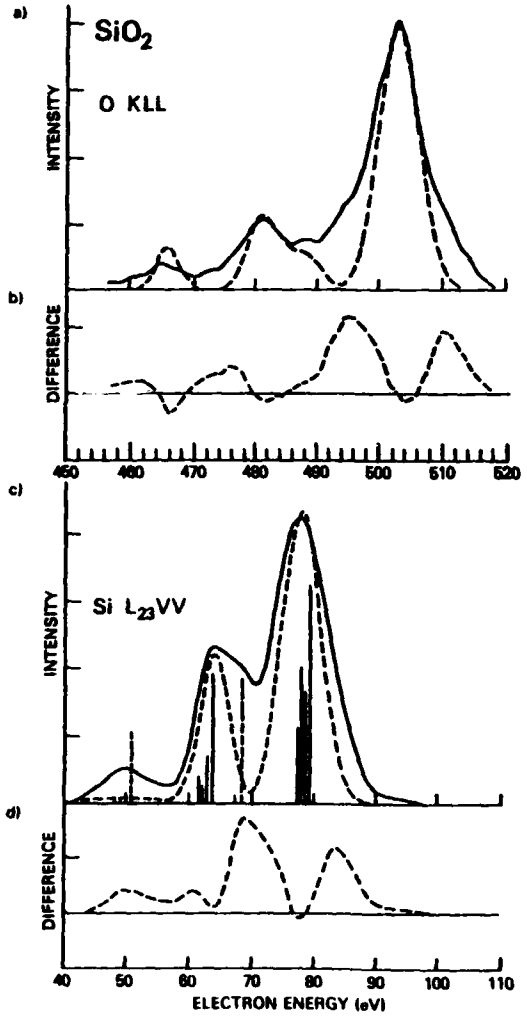
a)
SiO_2
O KLL
INTENSITY
b)
DIFFERENCE
450
460
470
480
490
500
510
520
c)
Si $L_{23}VV$
INTENSITY
d)
DIFFERENCE
40
50
60
70
80
90
100
110
ELECTRON ENERGY (eV)

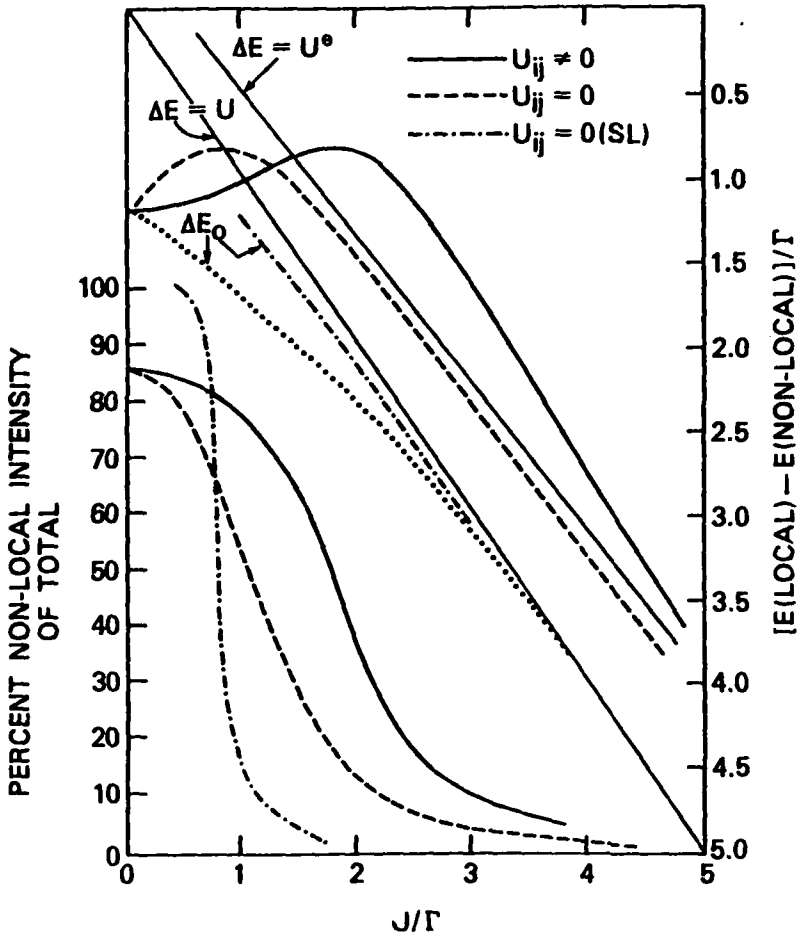
$\Delta E = U^e$
$\Delta E = U$
ΔE_0
$U_{ij} \neq 0$
$U_{ij} = 0$
$U_{ij} = 0$(SL)
PERCENT NON-LOCAL INTENSITY OF TOTAL
[E(LOCAL) − E(NON-LOCAL)]/Γ
J/Γ
0
10
20
30
40
50
60
70
80
90
100
0.5
1.0
1.5
2.0
2.5
3.0
3.5
4.0
4.5
5.0
1
2
3
4
5

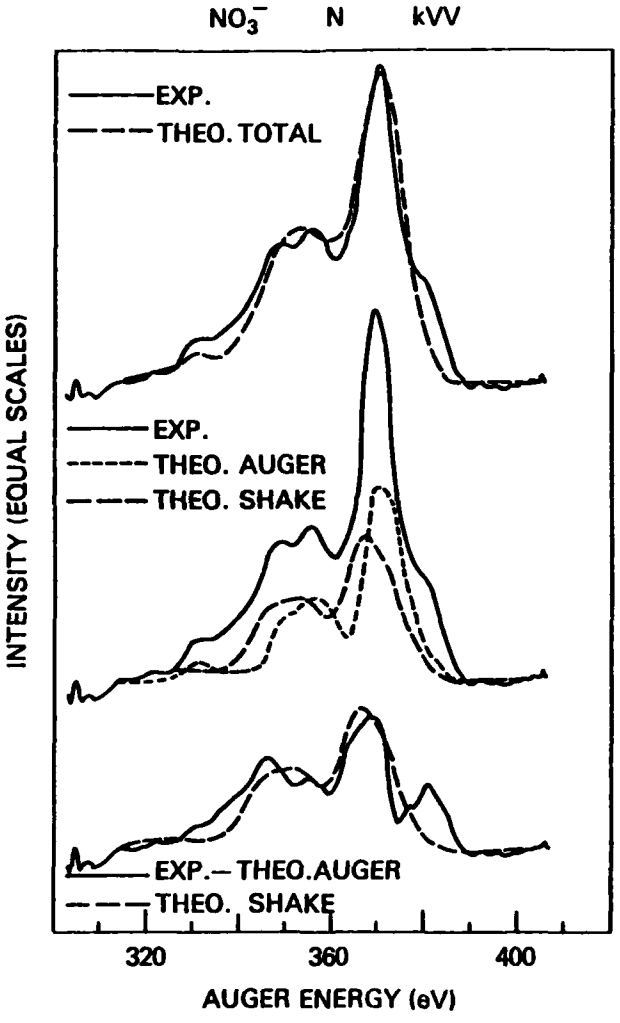
NO_3^- N kVV
EXP.
THEO. TOTAL
EXP.
THEO. AUGER
THEO. SHAKE
EXP.—THEO.AUGER
THEO. SHAKE
INTENSITY (EQUAL SCALES)
320
360
400
AUGER ENERGY (eV)

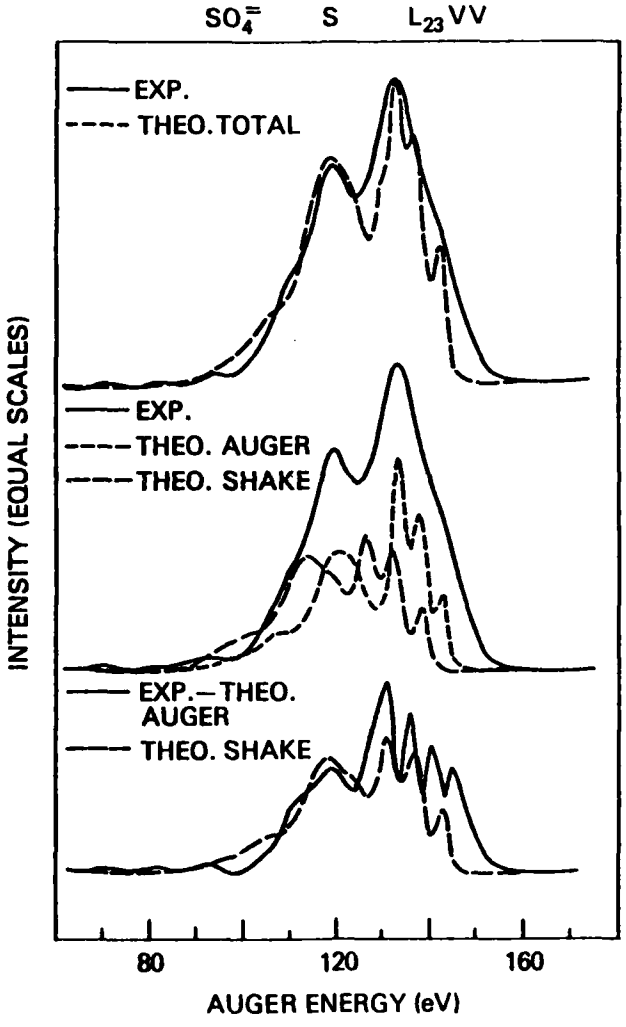
$SO_4^=$ S $L_{23}VV$
EXP.
THEO.TOTAL
EXP.
THEO. AUGER
THEO. SHAKE
EXP.—THEO. AUGER
THEO. SHAKE
INTENSITY (EQUAL SCALES)
80
120
160
AUGER ENERGY (eV)

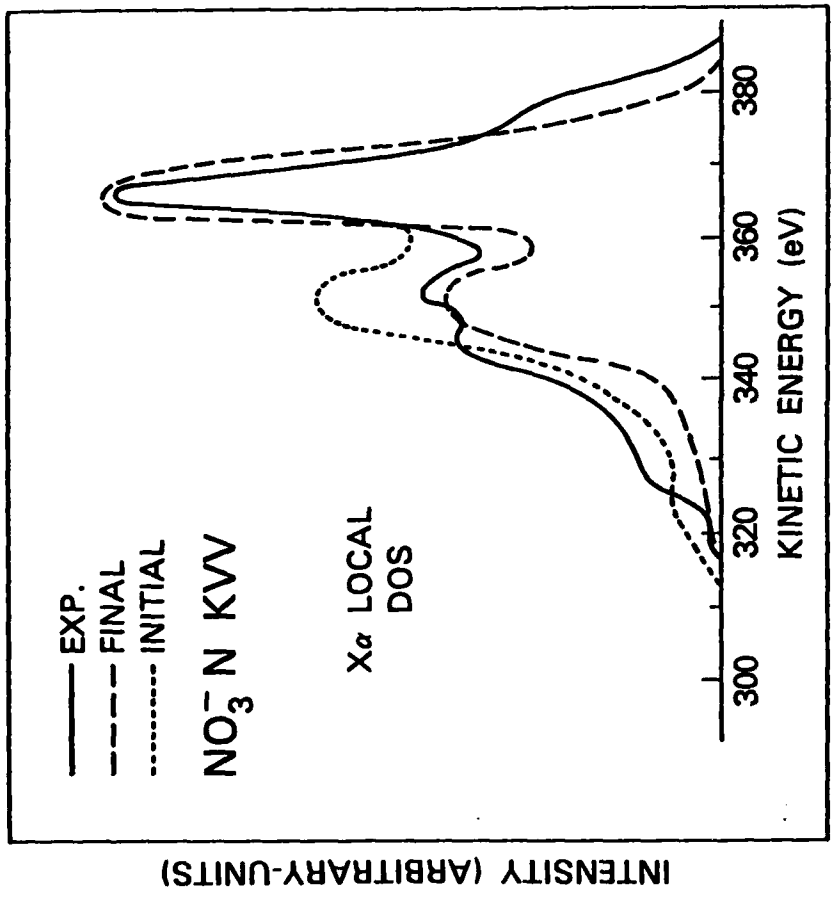
EXP.
FINAL
INITIAL
NO_3^- N KVV
Xα LOCAL DOS
300
320
340
360
380
KINETIC ENERGY (eV)
INTENSITY (ARBITRARY-UNITS)

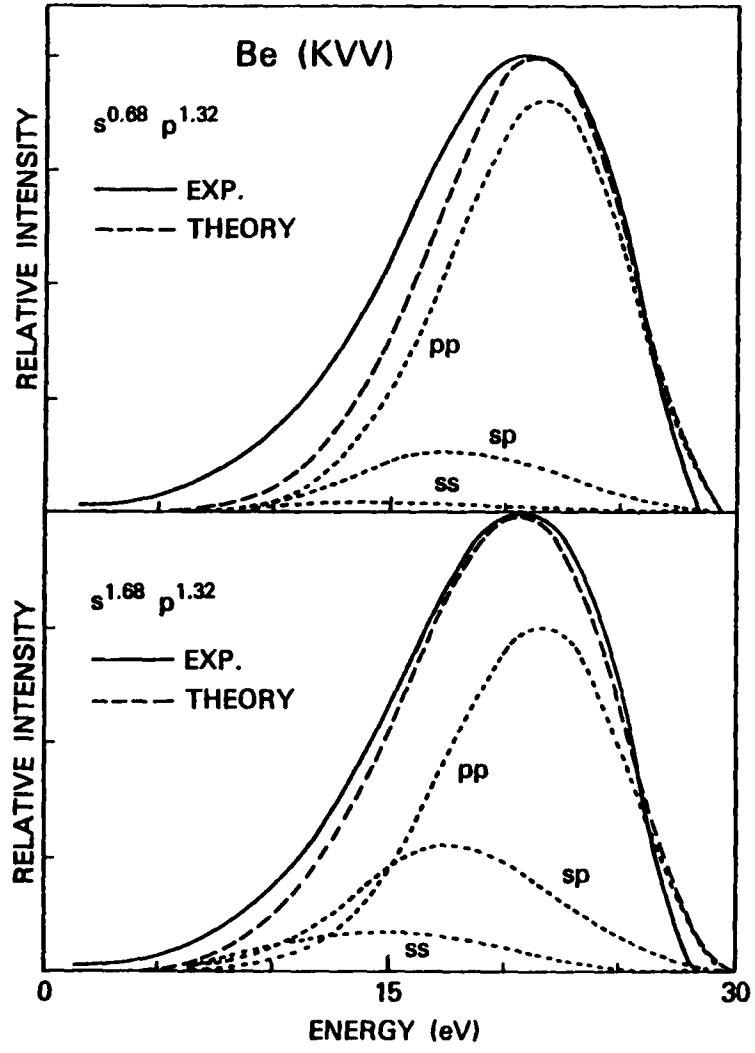
Be (KVV)
$s^{0.68}$ $p^{1.32}$
EXP.
THEORY
pp
sp
ss
RELATIVE INTENSITY
$s^{1.68}$ $p^{1.32}$
EXP.
THEORY
pp
sp
ss
RELATIVE INTENSITY
0
15
30
ENERGY (eV)

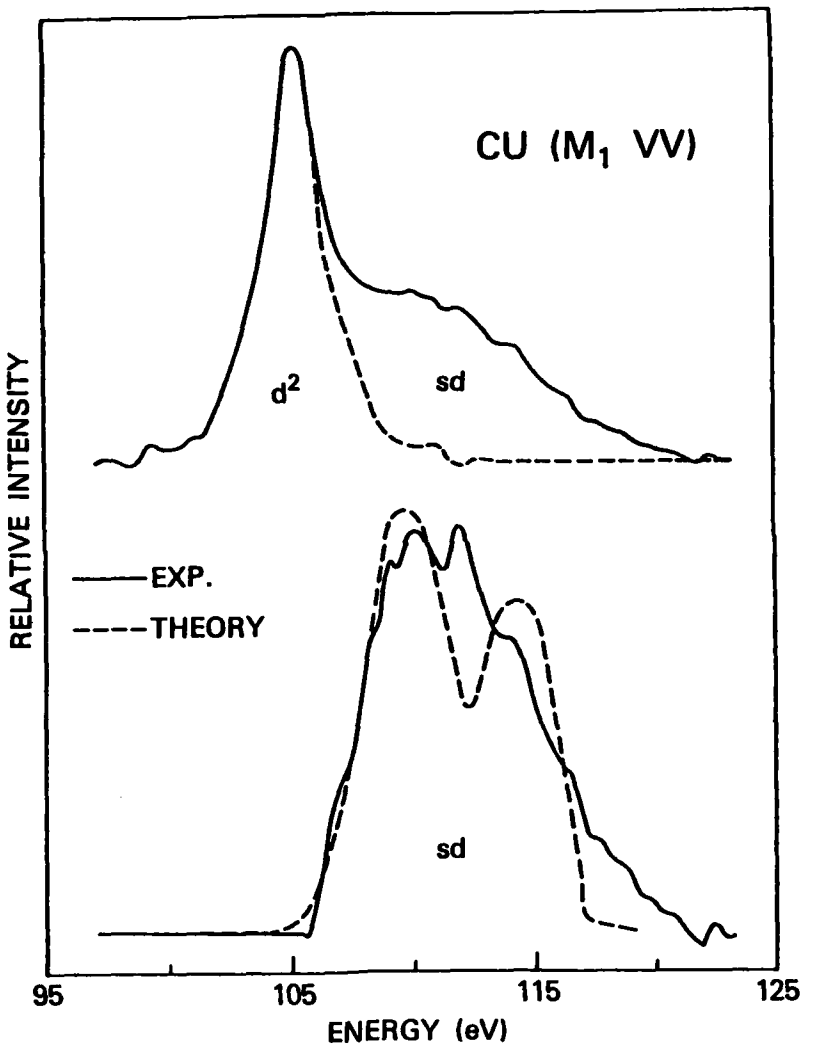
CU (M_1 VV)
d^2
sd
EXP.
THEORY
sd
RELATIVE INTENSITY
95
105
115
125
ENERGY (eV)

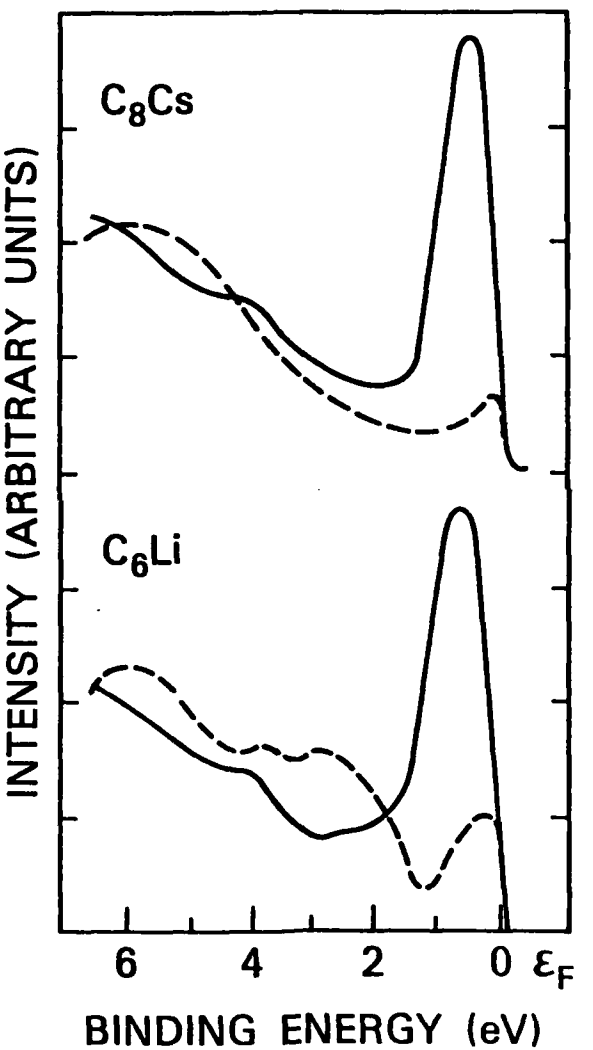
C_8Cs
C_6Li
INTENSITY (ARBITRARY UNITS)
6
4
2
0
ε_F
BINDING ENERGY (eV)

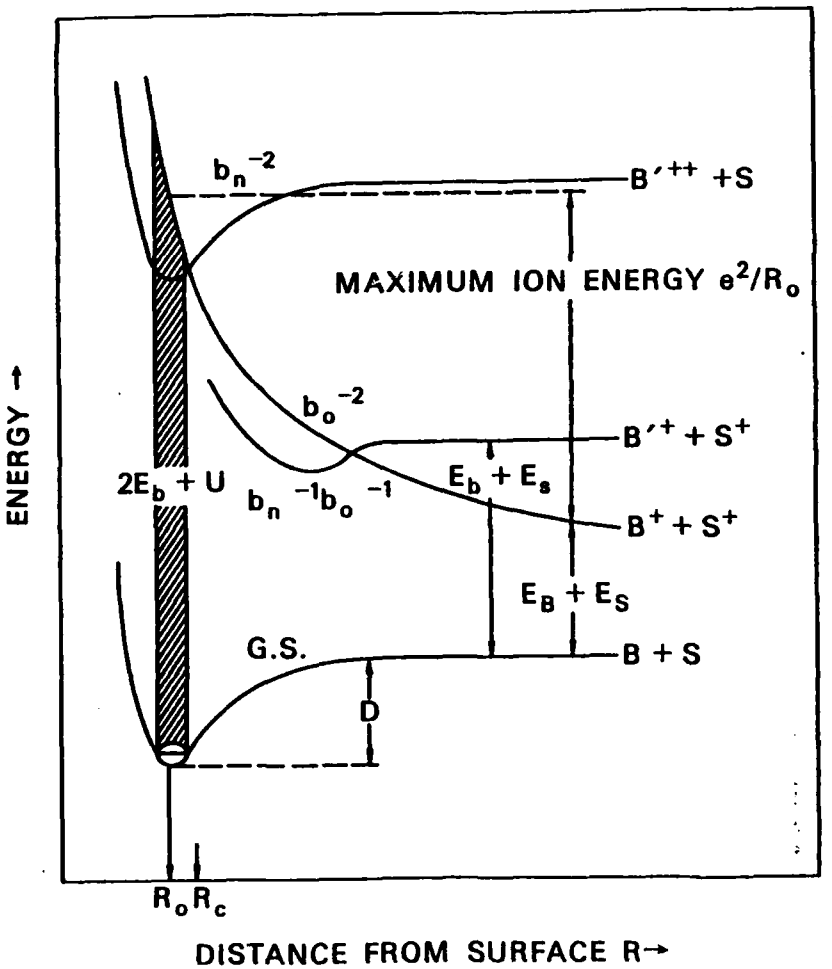
ENERGY →
b_n^{-2}
$B'^{++} + S$
MAXIMUM ION ENERGY e^2/R_o
b_o^{-2}
$B'^{+} + S^{+}$
$2E_b + U$
$b_n^{-1} b_o^{-1}$
$E_b + E_s$
$B^{+} + S^{+}$
$E_B + E_S$
G.S.
$B + S$
D
R_o R_c
DISTANCE FROM SURFACE R→

15

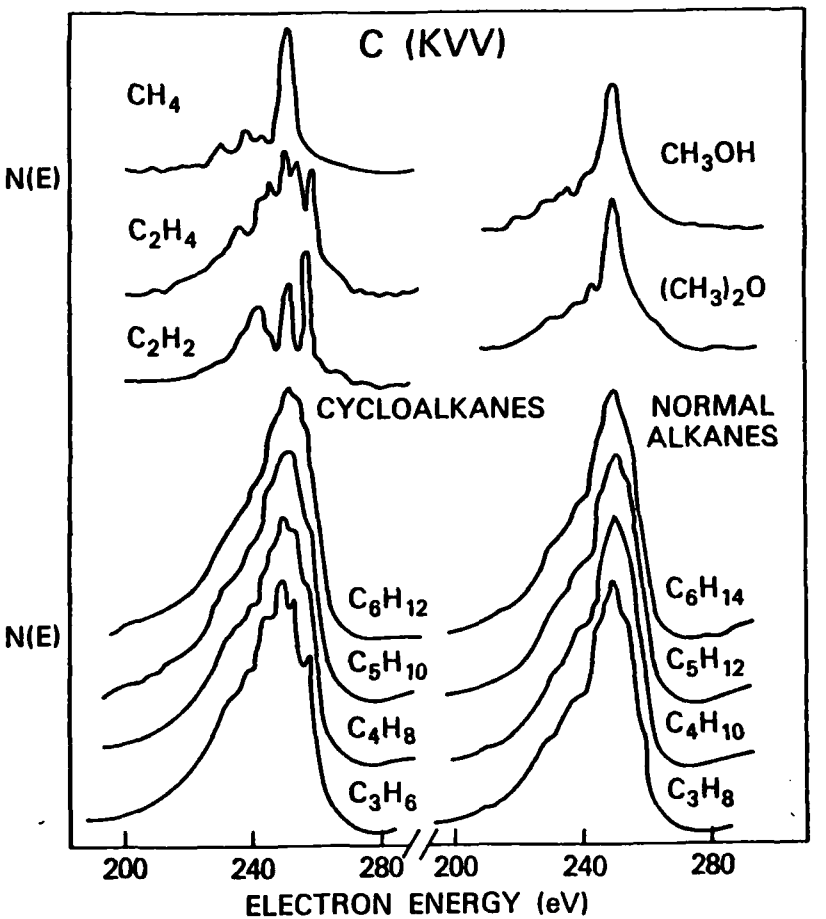
C (KVV)
CH_4
C_2H_4
C_2H_2
CH_3OH
$(CH_3)_2O$
N(E)
CYCLOALKANES
NORMAL ALKANES
C_6H_{12}
C_5H_{10}
C_4H_8
C_3H_6
C_6H_{14}
C_5H_{12}
C_4H_{10}
C_3H_8
N(E)
200
240
280
200
240
280
ELECTRON ENERGY (eV)

16

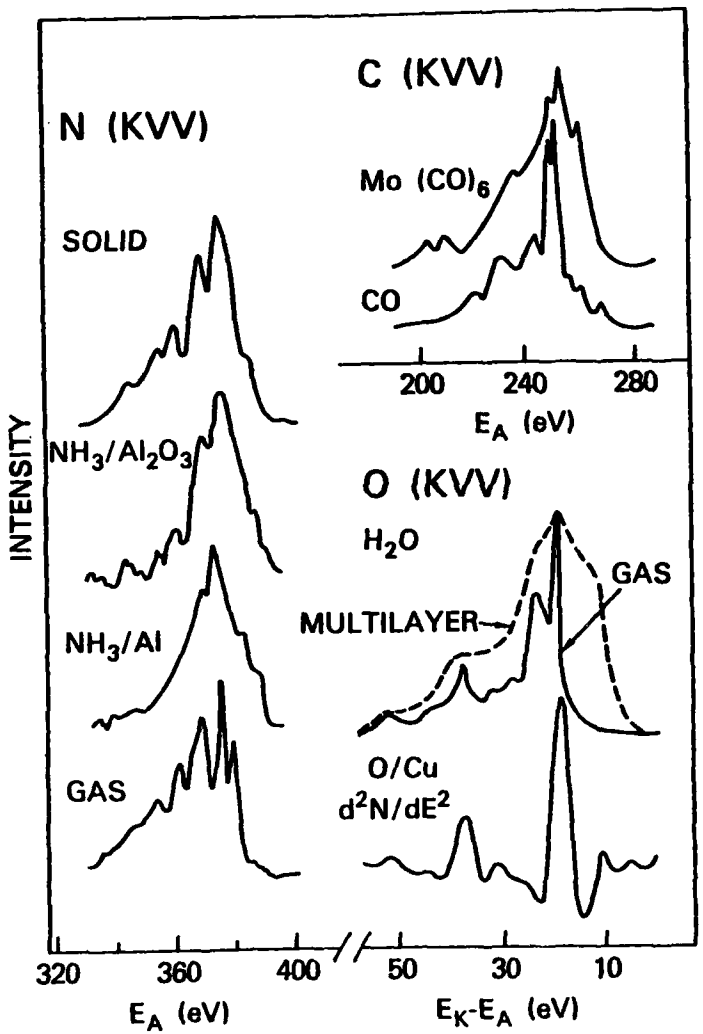
N (KVV)
SOLID
NH_3/Al_2O_3
NH_3/Al
GAS
INTENSITY
320
360
400
E_A (eV)
C (KVV)
$Mo(CO)_6$
CO
200
240
280
E_A (eV)
O (KVV)
H_2O
GAS
MULTILAYER
O/Cu
d^2N/dE^2
50
30
10
E_K-E_A (eV)

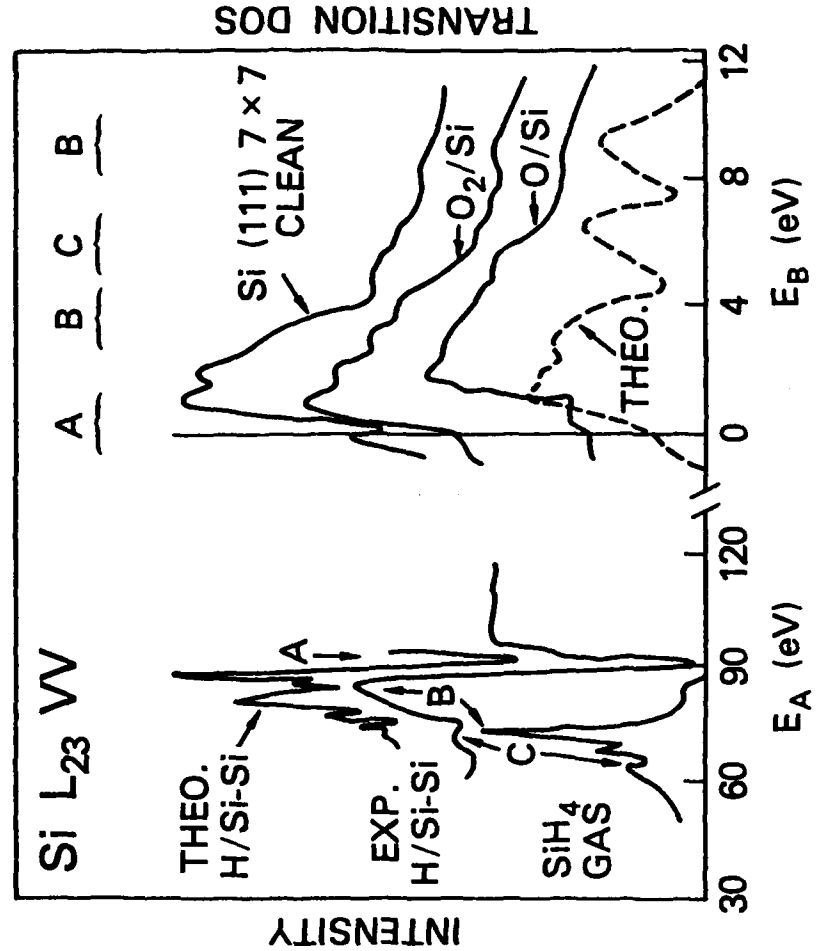
TRANSITION DOS
A
B
C
B
Si (111) 7 × 7
CLEAN
O_2/Si
O/Si
THEO.
12
8
4
0
E_B (eV)
Si L_{23} VV
A
B
C
THEO.
H/Si-Si
EXP.
H/Si-Si
SiH_4
GAS
120
90
60
30
E_A (eV)
INTENSITY

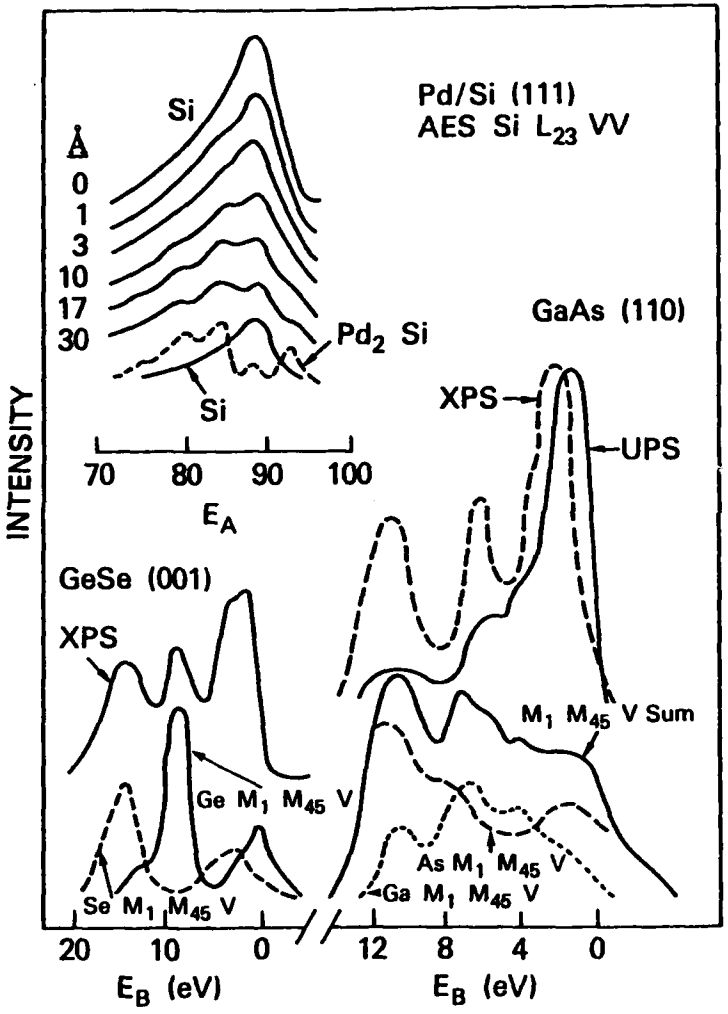
Pd/Si (111)
AES Si L_{23} VV
Si
Å
0
1
3
10
17
30
Pd_2 Si
Si
70
80
90
100
E_A
GaAs (110)
XPS
UPS
INTENSITY
GeSe (001)
XPS
Ge M_1 M_{45} V
Se M_1 M_{45} V
M_1 M_{45} V Sum
As M_1 M_{45} V
Ga M_1 M_{45} V
20
10
0
12
8
4
0
E_B (eV)
E_B (eV)

	No. Copies
Dr. S. Sibener Department of Chemistry James Franck Institute 5640 Ellis Avenue Chicago, Illinois 60637	1
Dr. M. G. Lagally Department of Metallurgical and Mining Engineering University of Wisconsin Madison, Wisconsin 53706	1
Dr. Robert Gomer Department of Chemistry James Franck Institute 5640 Ellis Avenue Chicago, Illinois 60637	1
Dr. R. G. Wallis Department of Physics University of California, Irvine Irvine, California 92664	1
Dr. D. Ramaker Chemistry Department George Washington University Washington, D.C. 20052	1
Dr. P. Hansma Chemistry Department University of California, Santa Barbara Santa Barbara, California 93106	1
Dr. P. Hendra Chemistry Department Southampton University England SO9JNH	1
Professor P. Skell Chemistry Department Pennsylvania State University University Park, Pennsylvania 16802	1
Dr. J. C. Hemminger Chemistry Department University of California, Irvine Irvine, California 92717	1
Dr. Martin Fleischmann Department of Chemistry Southampton University Southampton SO9 5NH Hampshire, England	1
Dr. J. Osteryoung Chemistry Department State University of New York at Buffalo Buffalo, New York 14214	1
Dr. G. Rubloff I.B.M. Thomas J. Watson Research Center P. O. Box 218 Yorktown Heights, New York 10598	1
Dr. J. A. Gardner Department of Physics Oregon State University Corvallis, Oregon 97331	1
Dr. G. D. Stein Mechanical Engineering Department Northwestern University Evanston, Illinois 60201	1
Dr. K. G. Spears Chemistry Department Northwestern University Evanston, Illinois 60201	1
Dr. R. W. Plummer University of Pennsylvania Department of Physics Philadelphia, Pennsylvania 19104	1
Dr. E. Yeager Department of Chemistry Case Western Reserve University Cleveland, Ohio 41106	2
Professor D. Hercules University of Pittsburgh Chemistry Department Pittsburgh, Pennsylvania 15260	1

TECHNICAL REPORT DISTRIBUTION LIST, 056

	No. Copies
Professor N. Winograd The Pennsylvania State University Department of Chemistry University Park, Pennsylvania 16802	1
Professor T. F. George The University of Rochester Chemistry Department Rochester, New York 14627	1
Professor Dudley R. Herschbach Harvard College Office for Research Contracts 1350 Massachusetts Avenue Cambridge, Massachusetts 02138	1
Professor Horia Metiu University of California, Santa Barbara Chemistry Department Santa Barbara, California 93106	1
Professor A. Steckl Rensselaer Polytechnic Institute Department of Electrical and Systems Engineering Integrated Circuits Laboratories Troy, New York 12181	1
Professor R. D. Archer University of Massachusetts Chemistry Department Amherst, Massachusetts 01003	1
Dr. A. C. Pastor Hughes Research Laboratories 3011 Malibu Canyon Road Malibu, California 90265	1

TECHNICAL REPORT DISTRIBUTION LIST, GEN

	No. Copies
Office of Naval Research Attn: Code 472 800 North Quincy Street Arlington, Virginia 22217	2
ONR Western Regional Office Attn: Dr. R. J. Marcus 1030 East Green Street Pasadena, California 91106	1
ONR Eastern Regional Office Attn: Dr. L. H. Peebles Building 114, Section D 666 Summer Street Boston, Massachusetts 02210	1
Director, Naval Research Laboratory Attn: Code 6100 Washington, D.C. 20390	1
The Assistant Secretary of the Navy (RE&S) Department of the Navy Room 4E736, Pentagon Washington, D.C. 20350	1
Commander, Naval Air Systems Command Attn: Code 310C (H. Rosenwasser) Department of the Navy Washington, D.C. 20360	1
Defense Technical Information Center Building 5, Cameron Station Alexandria, Virginia 22314	12
Dr. Fred Saalfeld Chemistry Division, Code 6100 Naval Research Laboratory Washington, D.C. 20375	1
U.S. Army Research Office Attn: CRD-AA-IP P.O. Box 1211 Research Triangle Park, N.C. 27709	1
Naval Ocean Systems Center Attn: Mr. Joe McCartney San Diego, California 92152	1
Naval Weapons Center Attn: Dr. A. B. Amster, Chemistry Division China Lake, California 93555	1
Naval Civil Engineering Laboratory Attn: Dr. R. W. Drisko Port Hueneme, California 93401	1
Department of Physics & Chemistry Naval Postgraduate School Monterey, California 93940	1
Scientific Advisor Commandant of the Marine Corps (Code RD-1) Washington, D.C. 20380	1
Naval Ship Research and Development Center Attn: Dr. G. Bosmajian, Applied Chemistry Division Annapolis, Maryland 21401	1
Naval Ocean Systems Center Attn: Dr. S. Yamamoto, Marine Sciences Division San Diego, California 91232	1
Mr. John Boyle Materials Branch Naval Ship Engineering Center Philadelphia, Pennsylvania 19112	1

TECHNICAL REPORT DISTRIBUTION LIST, 056

	No. Copies
Dr. G. A. Somorjai Department of Chemistry University of California Berkeley, California 94720	1
Dr. L. N. Jarvis Surface Chemistry Division 4555 Overlook Avenue, S.W. Washington, D.C. 20375	1
Dr. J. B. Hudson Materials Division Rensselaer Polytechnic Institute Troy, New York 12181	1
Dr. John T. Yates Surface Chemistry Section National Bureau of Standards Department of Commerce Washington, D.C. 20234	1
Dr. Theodore E. Madey Surface Chemistry Section Department of Commerce National Bureau of Standards Washington, D.C. 20234	1
Dr. J. M. White Department of Chemistry University of Texas Austin, Texas 78712	1
Dr. Keith H. Johnson Department of Metallurgy and Materials Science Massachusetts Institute of Technology Cambridge, Massachusetts 02139	1
Dr. J. E. Demuth IBM Corporation Thomas J. Watson Research Center P.O. Box 218 Yorktown Heights, New York 10598	1
Dr. C. P. Flynn Department of Physics University of Illinois Urbana, Illinois 61801	1
Dr. W. Kohn Department of Physics University of California (San Diego) LaJolla, California 92037	1
Dr. R. L. Park Director, Center of Materials Research University of Maryland College Park, Maryland 20742	1
Dr. W. T. Peria Electrical Engineering Department University of Minnesota Minneapolis, Minnesota 55455	1
Dr. Chia-wei Woo Department of Physics Northwestern University Evanston, Illinois 60201	1
Dr. D. C. Mattis Polytechnic Institute of New York 333 Jay Street Brooklyn, New York 11201	1
Dr. Robert M. Hexter Department of Chemistry University of Minnesota Minneapolis, Minnesota 55455	1
Dr. R. P. Van Duyne Chemistry Department Northwestern University Evanston, Illinois 60201	1